Stem Cell Research & Therapy

RESEARCH

Open Access

hAMSCs regulate EMT in the progression of experimental pulmonary fibrosis through delivering miR-181a-5p targeting TGFBR1

Yanyang Wang[1,2], Chan Liu[1,2], Nuoxin Wang[1,2], Dong Weng[1,2], Yan Zhao[3], Hongyu Yang[1,2], Haoyuan Wang[4], Shangfu Xu[1,2], Jianmei Gao[5], Changhui Lang[6], Zhenhai Fan[1,2], Limei Yu[1,2] and Zhixu He[7,8*]

Abstract

Background Pulmonary fibrosis (PF) is a common and multidimensional devastating interstitial lung disease. The development of novel and more effective interventions for PF is an urgent clinical need. A previous study has found that miR-181a-5p plays an important role in the development of PF, and human amniotic mesenchymal stem cells (hAMSCs) exert potent therapeutic potential on PF. However, whether hAMSCs act on PF by delivering miR-181a-5p and its detailed mechanism still remain unknown. Thus, this study was designed to investigate the underlying possible mechanism of hAMSCs on PF in bleomycin (BLM)-induced mouse PF model, and a co-culture system of hAMSCs and A549 cells epithelial mesenchymal transition (EMT) model, focusing on its effects on collagen deposition, EMT, and epithelial cell cycle regulation.

Methods hAMSCs with different miR-181a-5p expression levels were constructed. BLM (4 mg/kg) was used to create a PF model, while TGF-β1 was used to induce A549 cells to construct an EMT model. Furthermore, the effects of different miR-181a-5p expression in hAMSCs on collagen deposition and EMT during lung fibrosis were assessed in *vivo* and in *vitro*.

Results We found that hAMSCs exerted anti-fibrotic effect in BLM-induced mouse PF model. Moreover, hAMSCs also exerted protective effect on TGFβ1-induced A549 cell EMT model. Furthermore, hAMSCs ameliorated PF by promoting epithelial cell proliferation, reducing epithelial cell apoptosis, and attenuating EMT of epithelial cells through paracrine effects. hAMSCs regulated EMT in PF through delivering miR-181a-5p targeting TGFBR1.

Conclusions Our findings reveal for the first time that hAMSCs inhibit PF by promoting epithelial cell proliferation, reducing epithelial cell apoptosis, and attenuating EMT. Mechanistically, the therapeutic effect of hMASCs on PF is achieved through delivering miR-181a-5p targeting TGFBR1.

Keywords Amniotic membrane mesenchymal stem cells, hAMSCs, Pulmonary fibrosis, Epithelial mesenchymal transition, miR-181a-5p, TGFBR1

*Correspondence:
Zhixu He
hzx@gmc.edu.cn
Full list of author information is available at the end of the article

Background

Pulmonary fibrosis (PF), also referred to as interstitial fibrosis, is a common interstitial lung disease of the respiratory system. Its etiology is associated with pathogenic microbial infections, long-term inhalation of hazardous substances, radiological injuries, autoimmune diseases, and genetic factors [1–4]. The available treatment for PF includes respiratory support, pulmonary rehabilitation training, and other non-pharmacological treatments, such as cough suppressants, analgesics, and other supportive therapeutic drugs, as well as anti-fibrotic drugs, such as antioxidants and immunosuppressive drugs; and lung transplantation for patients with end-stage fibrosis [5–7]. However, these treatments cannot inhibit fibrosis or promote damage repair. Even after lung transplantation, the five-year survival rate is only 50–56% [2, 8]. Since the outbreak of SARS, H1N9, and novel coronavirus pneumonia, interstitial fibrosis in patients with a long disease course or high incidence of interstitial fibrosis after healing has become a major health challenge that affects cardiopulmonary function and quality of life [9–11]. This necessitates novel interventions for PF.

Mechanisms involved in the development of PF include (1) alteration of the immune environment: immune cell populations, such as macrophages and T-cells, contribute to the alteration of the immune environment following lung epithelial injury by secreting pro-fibrotic transmitters such as inflammatory factors and immunoreactive substances [4, 12–14]; (2) Increase in fibroblast production: in addition to the lung fibroblasts (resident fibroblasts and circulating fibroblast-like cells) proliferation and migration, damaged lung epithelial cells are a source of fibroblasts through epithelial mesenchymal transition (EMT)[15–18]. (3) Apoptosis of epithelial cells: during the development of PF, alveolar epithelial cells also undergo apoptosis [19, 20]. (4) Neovascularization: during the development of fibrosis, extensive neovascularization occurs in the neoplastic region of fibrosis. The production of angiogenic factors, such as vascular endothelial growth factor and angiogenic chemokines, is closely related to PF and associated with increased lung fibrosis [21, 22]. These factors promote myofibroblast production, collagen generation, and interstitial deposition, ultimately leading to interstitial lung fibrosis [23]. Therefore, in addition to effectively relieving the primary etiology, early intervention to inhibit the inflammatory response, suppress EMT, and attenuate epithelial cell apoptosis is the key to treating PF.

The TGF-β1/TGFBR1 axis plays an important role in fibrosis and the therapeutic mechanism of fibrosis [24–28]. TGF-β1 can regulate the differentiation of various immune-related cells such as CD8 + T cells, Treg and NK-T cells, and T cell helper cells to promote fibrogenesis through TGFBR1 [29]. TGF-β1 has also been shown to initiate downstream transcriptional regulation by activating TGFBR1, leading to the development of EMT [30–32]. Regarding the specific mechanism of action, TGF-β1/TGFBR1 regulates the JAK/STAT, Smad, MAPK, Wnt, and ERK pathways that play an important role in the development of PF [33].

Mesenchymal stem cells (MSCs) from different sources have demonstrated therapeutic effects on PF through their anti-apoptotic, anti-inflammatory, and anti-oxidative stress properties [23, 34, 35]. miRNAs are a class of non-coding RNAs that can alter the binding of target mRNAs by altering their pathway and mechanism of action, and are key paracrine information molecules in the function of MSCs, have received research attention [36–39]. miRNAs affect key physiological and pathological processes [40] and are involved in inflammatory and fibrotic processes, bone marrow stem cells, and other tissues [41, 42]. MSCs can interfere with inflammation and fibrosis by delivering miRNAs, bone marrow MSCs can attenuate lipopolysaccharide-induced acute lung injury and fibrosis by delivering miR-182-5p [41], and miR-186 can block fibroblast activation and ameliorate PF by delivering miR-186 to act on SOX4 and DKK1 [42]. miR-181a/b can inhibit inflammation and ameliorate pulmonary arterial hypertension. miR-181a-5p has been demonstrated to reduce renal fibrosis by directly targeting TGFBR1[43, 44]. Human amniotic mesenchymal stem cells (hAMSCs), compared with other sources of MSCs, are abundant in the amniotic membrane tissue, easily accessible, and have low immunogenicity and significant anti-inflammatory effects [45–47]. hMASCs have been reported to have significant therapeutic effects on PF caused by paraquat poisoning and can improve lung histopathological changes and reduce collagen deposition by reducing the expression of inflammatory cytokines, such as TGF-β1 [48]. In a previous study using the miGator database, the expression of miR-181a-5p was high in lung tissues and stem cells and reduced in the lung tissues of mice with PF, suggesting that miR-181a-5p plays an important role in the development of PF and the therapeutic effect of hMASCs on PF.

The dual-luciferase report verified the miR-181a-5p targeted binding to TGFBR1. Considering the role of TGFBR1 in PF, the following question remains to be addressed: Do hAMSCs act on PF by delivering miR-181a-5p to target TGFBR1?

Based on above-mentioned scenario, bleomycin (BLM)-induced mouse PF model, and a co-culture system of hAMSCs and A549 cells EMT model were used to investigate the effect of hAMSCs on PF and further explore its underlying possible mechanism. This will provide a new theoretical basis for the investigation of the

specific mechanism of hAMSCs in the treatment of PF, and offer an insight into the early use of hAMSCs in the treatment of PF in clinic.

Methods

Animals

The work has been reported in line with the ARRIVE guidelines 2.0. Healthy male C57BL/6 mice of 6–8 weeks of age were purchased from Hunan Slake Kingda Laboratory Animal Co. All mice were caged in a 12 h light/dark cycle standard condition, the temperature 22 ± 2 °C and the 55%–60% humidity with free access to standard rodent diet and sterile water. The experimental animals used in this study were in strict compliance with the 3Rs principle, and the experimental animals and operation procedures were in accordance with the regulations on the management of experimental animals issued by the Laboratory Animal Welfare AND Ethics Committee of Zunyi Medical University (No. ZMU22-2203-022), and the experimental procedures were performed according to the National Institutes of Health guide for the care and use of Laboratory animals (NIH Publications No. 8023, revised 1978).

Cell culture

Collection and culture of hAMSCs were performed and approved by the Ethics Committee of Zunyi Medical University (ZMU2022-1–142). After obtaining informed consent from the mothers and their families and conducting prenatal checkups to exclude hepatitis B, hepatitis C, HIV infection, and mothers over the age of 35 years, uncontaminated placental amniotic membranes from full-term cesarean deliveries were aseptically collected, placed in sterile saline solution, and transferred to the laboratory. The hAMSCs were extracted using the established laboratory method. hAMSCs were cultured in Low glucose Dulbecco's Modified Eagle Medium (LG-DMEM) + 10% Fetal Bovine Serum (FBS) + L-glutamine + human Fibroblast Growth Factor (FGF) basic (10 ng/100 mL) in 37 °C and 5% CO_2. hAMSCs of the third to fifth generation were used in all experiments.

Human non-small cell lung cancer cell line (A549 cells) source and culture: A549 cells were purchased from Kunming Cell Bank of the Chinese Academy of Sciences. The medium used was DMEM/F12 + 10% FBS + 1% penicillin–streptomycin (P/S) mixture and the culture conditions were 37 °C and 5% CO_2.

Human embryonic renal cells 293 cells (293 T cells) source and culture: 293 T cell line was obtained from the CAS cell bank. The medium used was DMEM + 10% FBS, and the culture conditions were 37 °C and 5% CO_2.

Identification of hAMSCs

Osteogenic and lipogenic-induced differentiation hAMSCs were seeded in well plates, and osteogenic-induced differentiation was conducted according to the manufacturer's instructions. The formation of calcified bone nodules was assessed using alizarin red staining, photographing, and recording. Lipogenic differentiation was induced by Oil Red O staining, photographs were taken, and lipid droplet formation was recorded. Immunohistochemical staining of mesenchymal stromal cell marker VIMENTIN: hAMSCs were seeded in well plates, washed with PBS, treated with paraformaldehyde, treated with 0.5% Triton solution at room temperature, incubated with H_2O_2 solution at 37 °C, blocked with goat closed serum, incubated with primary antibody, stored overnight at 4 °C, incubated with biotin-labeled corresponding secondary antibody, incubated at 37 °C, configured with DAB chromogenic solution, DAB chromogenic solution was added dropwise to observe the staining changes, rinsed with running water, and hematoxylin staining was added to stain the nuclei, which were photographed for analysis. Determination of cell growth curve: hAMSCs were inoculated into 96-well plates and cultured for 1–7 days and incubated with CCK-8 solution to the corresponding well plates, the absorbance value at 450 nm (OD value) was determined using an enzyme marker, with the OD value as the vertical coordinate and the growth time as the horizontal coordinate and the growth curve of hAMSCs was plotted. hAMSCs were identified as phenotypes according to the kit instructions, CD44-PE was added into a flow-through tube with CD73-APC, CD90-FITC, and CD105-PerCP-Cy5.5 flow-through detection antibodies and their isotypes, and PE-labeled HLA-DR, CD11b, CD19, CD34, CD34, CD45 antibodies and their isotype controls, and the third-generation hAMSCs suspensions were added and incubated at 4 °C in the dark for 30 min. At the end of the incubation period, the sample was washed twice with PBS, resuspended in staining buffer, and analyzed using flow cytometry.

Bioinformatics analysis of miR-181a-5p

Genomic information: basic information on hsa-miR-181a-5p was retrieved from the online database UCSC (http://genomeasia.ucsc.ed), and the mature sequences of genes from different species were compared and analyzed. Expression levels in human tissues: The miRGator v3.0 database (http://mirgator.obic.re.kr/) was used to analyze hsa-miR-181a-5p and retrieve its expression levels of hsa-miR-181a-5p in different human tissues and organs. Target gene prediction and KEGG pathway enrichment: Three databases, miRWALK (http://

mirwalk.umm.uniheidelberg.de/), miRDB (http://www.mirdb.org/), and Target Scan (http://www.targetscan.org/vert71/), were used to predict the target genes of hsa-miR-181a-5p, and their intersecting target genes were used for subsequent analysis. The intersecting target genes of the three databases were used for KEGG signaling pathway enrichment analysis using the SangerBox database (http://sangerbox.com/home.html). hsa-miR-181a-5p was predicted to bind to the TGFBR1 binding site using the Target Scan (http://www.targetscan.org/vert71/) database for binding site prediction.

miR-181a-5p and TGFBR1 dual luciferase reporter assay

Experimental plasmids pMIR-REPORT Luciferase (H306, Obio Technology (Shanghai) Corp., Ltd.), pMIR-REPORT Luciferase-TGFBR1 3'UTR(WT) (H23650, Obio), pMIR-REPORT Luciferase-TGFBR1 3 ' UTR (hsa-miR-181a-5p MUT) (H23651, Obio)were used; primer sequences are listed in Table 1. The experiments were performed in strict accordance with the Obio protocol.

Transfection of hAMSCs with miR-181a-5p agomir, antagomir, and identification of relative expression of miR-181a-5p

One day before transfection, hAMSCs were inoculated in a six-well plate to achieve 30–50% confluence during transfection, and Lipofectamine 2000-agomir or Lipofectamine 2000-antagomir complexes were individually configured for each sample at different concentrations or groups and gently mixed before use. 5 μL Lipofectamine 2000 was added to 245 μL Opti-MEM medium, mixed gently, and incubated at room temperature for 5 min; 250 μL Opti-MEM medium was used to dilute miR-181a-5p agomir, miR-181a-5p antagomir configured according to the instructions (when added to the well plates, the final sample was mixed gently with Lipofectamine 2000-agomir or Lipofectamine 2000-antagomir complex), the final concentration when added to the plate was 50, 100, or 200 nM. The liquid was gently mixed from the first two steps to form a complex and incubated at room temperature for 20 min. The cells were washed in the well plate with PBS, the Opti-MEM medium was added, followed by the complex to the wells containing the cells. The total amount of liquid in each well was 2 mL, and the plate was gently shaking. The cells were incubated in a CO_2 incubator at 37 °C for 4–6 h and collected after 24–48 h and set aside. Extraction of total RNA: hAMSCs from different experimental groups were lysed with TRIzol reagent (Invitrogen), and mRNA was extracted with RNA isolation kit (Qiagen). Identification of transfection efficiency: After extraction of total RNA, miRNA first-strand cDNA synthesis was conducted, the reverse transcription system and reaction conditions were conducted in strict accordance with the instructions, and the reaction mixture was added to a centrifuge tube in an ice bath, gently mixed, and centrifuged for 3–5 s. The reaction took place in a 37 °C bath for 60 min, then heated to 85 °C for 5 min to inactivate the enzyme, and the samples obtained from the reaction were preserved at 4 °C. miRNA fluorescence PCR: The cDNA reaction solution was diluted 50 times and used. The miRNA fluorescence PCR amplification system and miRNA amplification conditions were performed according to the instruction manual, with predenaturation at 95 °C for 30 s, denaturation at 95 °C for 5 s, and annealing/extension at 60 °C for 30 s for a total of 40 cycles, and the dissolution curve was set according to the instrument. The primers used were synthesized by Shanghai Sangong Biotechnology Co., Ltd., according to the primer sequences provided by Obio, and the internal reference was U6. The relative expression levels of miRNAs were calculated using the $2^{-\Delta\Delta Ct}$ method (Table 2).

Table 1 Experimental primer sequences

Name	Sequence
H23650 TGFBR1 3'UTR (WT)	Luc-C-F GAGGAGTTGTGTTTGTGGAC M13F TGTAAAACGACGGCCAGT
H23651 TGFBR1 3'UTR (hsa-miR-181a-5p MUT)	Luc-C-F GAGGAGTTGTGTTTGTGGAC M13F TGTAAAACGACGGCCAGT

Grouping and treatment of animals

The work has been reported in line with the ARRIVE guidelines 2.0. The mice were divided, using a simple randomization method, into five groups (n = 4) treated as follows: control group: no treatment; lung fibrosis model group: one-time tracheal injection of 4 mg/kg BLM solution on day 0 of the experiment, and on day 7, each mouse was injected with 0.2 mL saline in the tail vein; the hAMSCs, AGO-hAMSCs, and ANTA-hAMSCs groups were given a one-time tracheal injection of 4 mg/kg BLM solution, and the different groups

Table 2 Transfected RNA oligo sequences and RT-qPCR primer sequences (tail method)

Name	Sequence(5′ to 3′)
miR-181a-5p agomir	S:AACAUUCAACGCUGUCGGUGAGU AS:UCACCGACAGCGUUGAAU GUUUU
miR-181a-5p agomir NC	S:UUCUCCGAACGUGUCACGUTT AS: ACGUGACACGUUCGGAGAATT
miR-181a-5p antagomir	S:ACUCACCGACAGCGUUGAAUGUU
miR-181a-5p antagomir NC	CAGUACUUUUGUGUAGUACAA
hsa-miR-181a-5p	AACAGTGAACATTCAACGCTGTC
mmu-miR-181a-5p	AACATTCAACGCTGTCGGTG

of mice were injected by tail vein injection of 0.2 mL of saline resuspended 5×10^5 hAMSCs, miR-181a-5p agomir-transfected hAMSCs (AGO-hAMSCs), and miR-181a-5p antagomir-transfected hAMSCs (ANTA-hAMSCs). hAMSCs were labeled using DiR dye after tail vein injection, 7 days after capturing in vivo fluorescent signals using in vivo imaging with a live imager. On day 28, all experimental mice were weighed, and their general state was observed and photographed. Lung tissues were extracted from experimental mice after being euthanized via cervical dislocation following anesthesia with inhalation of isoflurane. The lung index was calculated as the weight of the lungs divided by the total body weight of the mice. The lung tissues were extracted from the middle lobe portion of the left lungs, fixed in 10% formalin, and used for hematoxylin and eosin (HE) staining of the pathology, MASSON staining to observe the pathological structure, immunohistochemical and immunofluorescence staining to observe the relevant indices, and Western Blotting to detect protein levels.

Establishment of A549 cell EMT model and hAMSCs co-culture system

According to the existing literature [49–52], the concentration of TGFβ1 was set at 5 and 10 ng/mL and the treatment duration was 24 h and 48 h. The cells were divided into six groups: 24 h control group, 24 h-5 ng/mL TGFβ1 treatment group, 24 h-10 ng/mL TGFβ1 treatment group, 48 h control group, 48 h-5 ng/mL TGFβ1 treatment group, 48 h-10 ng/mL TGFβ1 treatment group; according to the literature [53–55], we selected two kinds of cell co-culture hAMSCs:A549 ratio of 1:1, 2:1, 5:1, respectively, and divided into the following five groups: control group, model group, co-culture1:1, co-culture2:1, co-culture5:1, and cell photographic observation with RT-qPCR, western blotting, and other methods to observe and analyze the cells relevant indicators. Finally, the co-culture system was divided into the following groups according to the results of the previous two steps: control group: no treatment; model group: treated with 5 ng/mL TGFβ1; hAMSCs co-culture group: treated with 5 ng/mL TGFβ1 for 24 h, hAMSCs were added into the Transwell, and the ratio of cells were hAMSCs:A549 = 1:1, co-culture for 48 h; AGO-hAMSCs co-culture group and ANTA-hAMSCs co-culture group were treated according to the above steps, and then 1:1 AGO-hAMSCs and ANTA-hAMSCs were added for co-culture, respectively.The control, model, and co-culture groups were subjected to an EdU proliferation assay, flow Annexin-FITC/PI staining, RT-qPCR, and western blotting to observe the relevant proliferation, apoptosis, and mesenchymalization indices.

Reverse transcription-quantitative polymerase chain reaction (RT-qPCR)

The total RNA extraction method followed the same procedure as described earlier. Reverse transcription after total RNA extraction: reverse transcription of RNA at adjusted concentrations was conducted according to the manufacturer's instructions, and the reaction solution was prepared on ice. Reaction conditions: After mixing the system, the reaction solution was prepared at 37 °C for 15 min (reverse transcription reaction), 85 °C for 5 s (inactivation reaction of reverse transcriptase), and stored at 4 °C. Amplification of target gene: amplify the cDNA in strict accordance with the system and conditions of the manual, the preparation of the reaction solution was carried out on ice. Reaction conditions: sample volume 25 μL, Step 1: 95 °C for 30 s, Step 2: PCR reaction GOTO:39(40 Cycles) 95 °C for 5 s, 60 °C for 30 s, Step 3: Melt Curve, primer sequences are shown in Table 3.

Cell transcriptome sequencing

Three stem cell co-culture groups (hAMSCs, AGO-hAMSCs, and ANTA-hAMSCs) were subjected to DNBSEQ eukaryotic transcriptome resequencing following the standard steps provided by the high-throughput laboratory of Wuhan Huada Genetic Technology Service Co. Ltd. Quality control was performed according to the "RNA Sequencing Sample Quality Standards", assessing RNA concentration, RIN/RQN, and 28S/18S ratios. The samples were analyzed using the DNBSEQ platform, reference species name: *Homosapiens*, source: NCBI, reference genome version: GCF_000001405.39_GRCh38.p13, and the raw data obtained from sequencing were filtered

Table 3 Primer sequences

Name	Sequence(5′ to 3′)
human GAPDH	F: CAGGAGGCATTGCTGATGAT R: GAAGGCTGGGGCTCATTT
human E-CAD	F: CTGGCGTCTGTAGGAAGG R: TCTTTGACCACCGCTCTC
human Cytokeratin	F: GATGAGCAGGTCCGAGGT R: GCCAGTGTGTCTTCCAAGG
human COL1A1	F: GTGCGATGACGTGATCTGTGA R: CGGTGGTTTCTTGGTCGGT
human N-CAD	F: GGACCATCACTCGGCTT R: GCAAACCTTCACACGCA
human VIMENTIN	F: CAGAGAGAGGAAGCCGAA R: TGCCAGAGACGCATTGT
human ZO-1	F: TGAGGCAGCTCACATAATGC R: GGGAGTTGGGGTTCATAGGT
human TGFBR1	F: TGTTGGTACCCAAGGAAAGC R: CACTCTGTGGTTTGGAGCAA
human BAX	F: ATGGACGGGTCCGGGG R: GGAAAAAGACCTCTCGGGGG

using SOAPnuke (v1.5.6) to obtain clean data. Dr. Tom's Multi-Organomics Data Mining System (https://biosys.bgi.com) was used for the data analysis, mapping, and mining. The clean data were compared with the reference genome using HISAT2 (v2.1.0) software and aligned to the reference gene set using Bowtie2 (v2.3.4.3). Gene expression was quantified using the RSEM (v1.3.1) software, and differential gene detection was performed using DESeq2 (v1.4.5). In the system, TPM was used as the reference to screen for reflecting differential folds; the hAMSCs co-culture group was set as the control group; the transcriptomic genes with $\log_2$ (expression in treatment group/expression in control group) differential expression were screened with a 1.5-fold difference in expression in the treatment group/expression in the control group at $P<0.05$, in which the AGO-hAMSCs co-culture group showed a 1.5-fold decrease in expression compared with the hAMSCs co-culture group and ANTA-hAMSCs co-culture group showed a 1.5-fold increase in expression compared with the hAMSCs co-culture group. The screened genes were further enriched for the KEGG pathway, heatmap was created to visualize the quantitative differences in expression levels of differentially expressed genes, and the standardization method was adopted as the z-score (row direction).

Statistical analysis

All data were expressed as mean ± standard deviation ($\bar{x} \pm s$), and the experimental data were statistically analyzed using the SPSS 29.0 (IBM Corp., Armonk, NY, USA, Version 29.0) software package, with the independent samples t-test for only two groups of data with quantitative information that satisfied the normal distribution, and one-way ANOVA for the mean of samples with three or more groups. If the differences were statistically significant, the LSD method was further used to compare the differences between groups, and the DunnettT3 test was chosen when the variance was not uniform, with $P<0.05$ suggesting statistical significance.

Results

Biological morphology and characterization of hAMSCs

Primary cultured hAMSCs showed a uniform morphology, were tightly arranged, and adhered to the plate bottom. P5 hAMSCs were long and spindle-shaped in a swirling arrangement, showing fibroblast morphology (Fig. 1A). P5 hAMSCs were induced by osteogenic induction and alizarin red staining, and a certain number of red alizarin red-stained calcium nodules were observed in the extracellular matrix (Fig. 1B). They were also induced by lipid induction and Oil Red O staining, and some red fat droplets were observed in the cytoplasm (Fig. 1C). Immunohistochemical staining of P5 hAMSCs for the mesenchymal cell marker VIMENTIN showed that the nuclei of cells in the negative control group were blue, and the cytoplasm was colorless (Fig. 1D). In contrast, the nuclei of cells in the stained group were blue, and the cytoplasm was brown (Fig. 1E). P5 hAMSCs were cultured for 7 days, and the cells showed exponential growth and strong cell proliferation on days 2–5 (Fig. 1F). Flow cytometry assay of the P5 hAMSCs showed that the cell surface positively expressed CD44 (99.97%), CD73 (99.97%), CD90 (99.95%), CD105 (97.49%), CD45, CD19, CD34, CD11b, and HLA-DR (0.22%) (Fig. 1G), which meets the International Society for Cell & Gene Therapy (ISCT) quality requirements for experimental MSCs: positive CD73, CD90, CD105 expression was > 95%, and the sum of CD45, CD19, CD34, CD11b and HLA-DR positive expression was < 2%.

Critical role of miR-181a-5p in pulmonary fibrosis, bioinformatics analysis related to miR-181a-5p, validation of the targeting relationship between miR-181a-5p and TGFBR1, transfection of hAMSCs with miR-181a-5p

As shown in Fig. 2A, the relative expression of miR-181a-5p in lung tissues of mice with PF was significantly lower than that of untreated mice ($P<0.01$), which suggested that the development of PF is accompanied by a decrease in miR-181a-5p. A search on the UCSC database revealed that the hsa-miR-181a-5p gene was localized between chromosome chr9:124,692,481–124,692,502 of the human genome. Analysis of the mature sequence of miR-181a-5p showed that the mature sequence of miR-181a-5p was basically consistent among species and highly conserved during species evolution(Fig. 2B). The expression of hsa-miR-181a-5p in human organs is shown in Fig. 2C. hsa-miR-181a-5p was highly expressed in human lungs and human-derived stem cells. A total of 8,112 target genes were predicted by miRWALK, 1408 by miRDB, 1,371 by Target Scan, and 483 by the intersection of the three databases. Meanwhile, 483 genes were enriched by the pathway. They were concentrated in the key pathway of lung fibrosis, namely the TGFβ signaling pathway, which encompasses the key gene for regulating lung fibrosis, TGFBR1, and is involved in vasoconstriction and inflammation. It also included the RAS signaling pathway, which is involved in vasoconstriction, inflammation, and fibrosis, as well as the MAPK, PI3K-AKT, and LONGEVITY REGULATING signaling pathways, which are involved in lifespan regulation, such as cell proliferation (Fig. 2D). As predicted by the TargetScan online database, hsa-miR-181a-5p is bound to the target gene TGFBR1 binding site (Fig. 2E). To verify whether TGFBR1 is the target gene of hsa-miR-181a-5p, a dual-luciferase reporter assay was performed, hsa-miR-181a-5p could regulate the

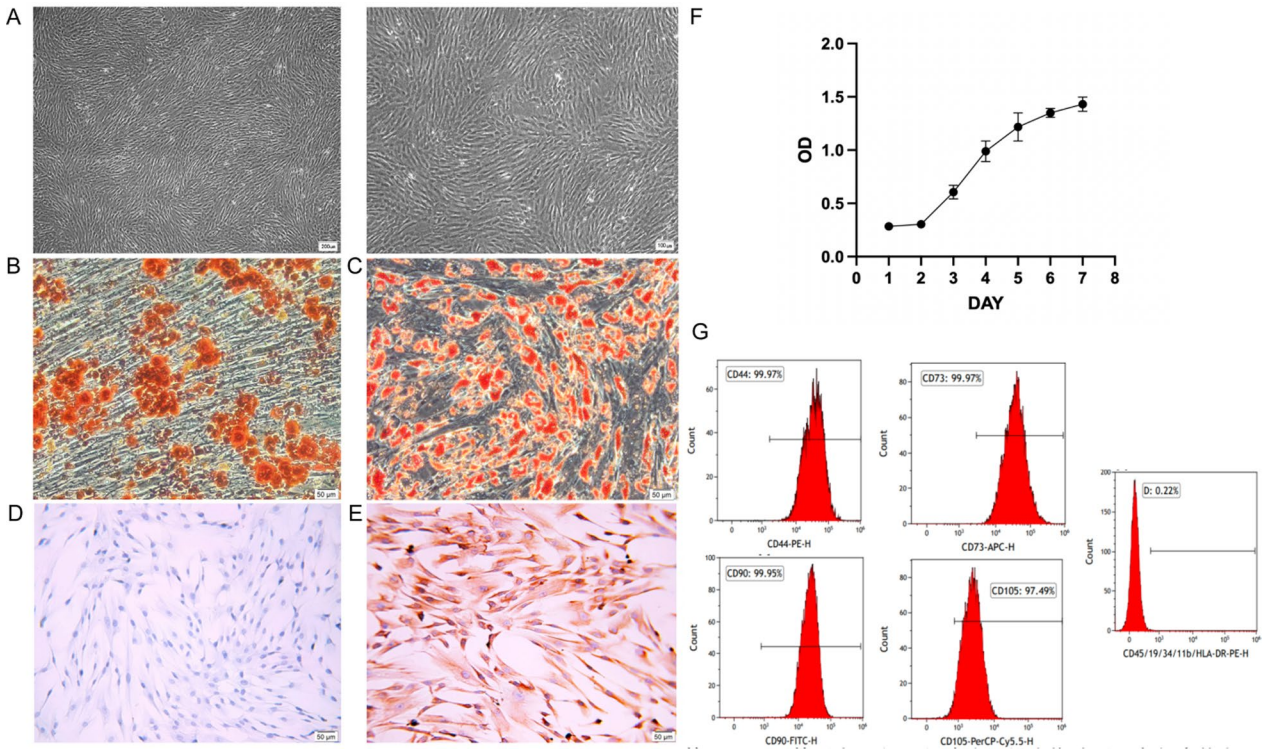

Fig. 1 Biological morphology and identification of hAMSCs. **A** Morphological observation of hAMSCs (scale bar = 200 μm, 100 μm). **B** Identification of osteogenic differentiation ability of hAMSCs (scale bar = 50 μm). **C** Identification of lipid differentiation ability of hAMSCs (scale bar = 50 μm). **D** Immunohistochemical identification of VIMENTIN, a surface marker of hAMSCs (scale bar = 50 μm). **E** Immunohistochemical identification of VIMENTIN, a surface marker of hAMSCs (scale bar = 50 μm). **F** Growth curve of hAMSCs (n = 3). **G** Identification of immunophenotypic surface markers of hAMSCs

expression of TGFBR1 luciferase with 3'UTR compared with the null-loaded group ($P < 0.05$). In the binding site mutation, this regulatory relationship disappeared, as shown in Fig. 2F, demonstrating the targeting relationship between hsa-miR-181a-5p and TGFBR1. Considering the key role of TGFBR1 in PF, miR-181a-5p may play an important role in the development and treatment of PF. The results of the miRNA fluorescence qPCR assay showed no statistically significant difference in transfection efficiency at an agomir concentration of 50 nM but a significant increase in the expression of hsa-miR-181a-5p at agomir transfection concentrations of 100 and 200 nM ($P < 0.001$ or $P < 0.0001$), as shown in Fig. 2G. There was no significant difference in transfection efficiency at an antagomir concentration of 50 nM; however, a significant decrease was observed in hsa-miR-181a-5p expression at antagomir transfection concentrations of 100 and 200 nM ($P < 0.001$ or $P < 0.0001$; Fig. 2H). Based on the product specification and the available literature, the final agomir selection concentration was 100 nM, and the antagomir selection concentration was 200 nM. AGO-hAMSCs transfected with 100 nM hsa-miR-181a-5p agomir showed a long shuttle-shaped adherent wall growth with ANTA-hAMSCs transfected with 200 nM hsa-miR-181a-5p antagomir, and the cell growth was good, indicating that the hAMSCs had a good transfection efficiency, while the cell growth status was not affected.

Effects of hAMSCs with different hsa-miR181a-5p expression levels on mice with pulmonary fibrosis

Figure 3A illustrates the time line of the animal experiments. During the modeling process, a visual tongue depressor was used to observe the opening and closing of the mouse glottis with respiratory movement. An atomized trachea injection needle was then inserted into the glottis to administer the modeling drug. Compared with traditional modeling methods, this approach allowed for visualization of the process (Fig. 3B). The mice had almost no choking response during the entire modeling process. Seven days after the injection of DIR-labeled hAMSCs into the tail vein, in vivo imaging of the animals showed that the hAMSCs were mainly concentrated in the lung tissue of mice, while some were in the liver tissue of mice (Fig. 3C). During the adaptive feeding phase before modeling, the body weight of mice in each group steadily increased. Within 7 days after modeling

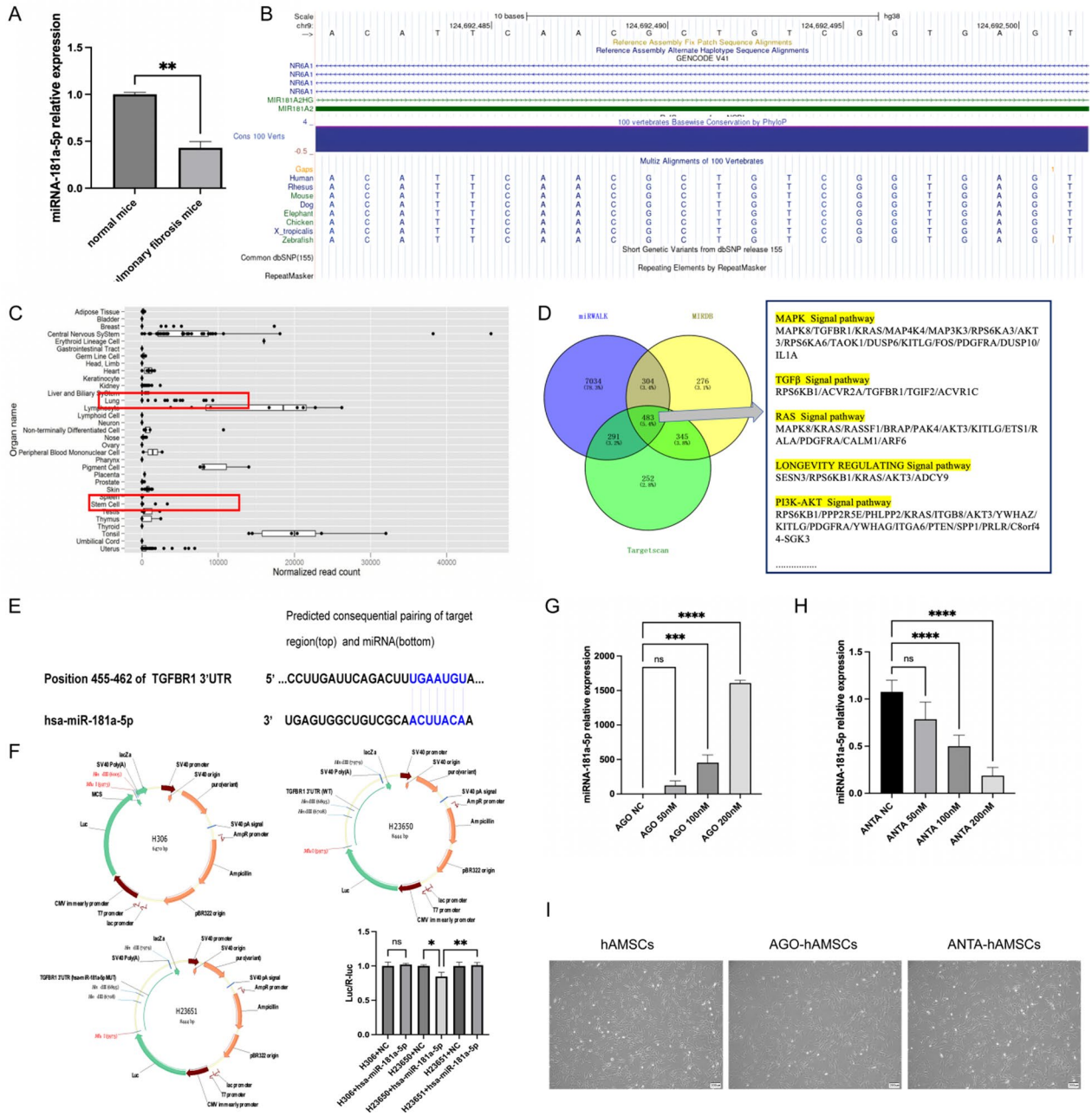

Fig. 2 Role of miR-181a-5p in PF. Bioinformatics analysis related to miR-181a-5p, validation of the targeting relationship between miR-181a-5p and TGFBR1, transfection of hAMSCs with miR-181a-5p. **A** Comparison of the expression level of miR181a-5p in lung tissues of normal mice and mice with PF ($\bar{x} \pm s$, n = 3) $^{**}P < 0.01$. **B** Gene localization of hsa-miR-181a-5p and the conserved mature sequences. **C** Expression of hsa-miR-181a-5p in various organs of the human body. **D** Prediction results of target genes of hsa-miR-181a-5p. **E** Target scan database prediction of the binding site of hsa-miR-181a-5p and TGFBR1. **F** Schematic diagram of plasmid construction and results of validation of dual luciferase reporter for the mutant site hsa-miR-181a-5p and TGFBR1. **G** hsa-miR-181a-5p agomir transfection concentration. H: hsa-miR-181a-5p antagomir transfection concentration ($\bar{x} \pm s$, n = 4). ns: $P > 0.05$, $^{***}P < 0.001$, $^{****}P < 0.0001$. I: Morphology of hAMSCs after hsa-miR-181a-5p transfection (scale bar = 200 μm)

(days 0–7), the body weight of mice in the blank control group increased steadily, and the body weight of mice in the lung fibrosis model and hAMSCs, AGO-hAMSCs, and ANTA-hAMSCs groups continued to decrease. On day 7 of stem cell treatment, the body weights of mice in the control group continued to increase steadily, those

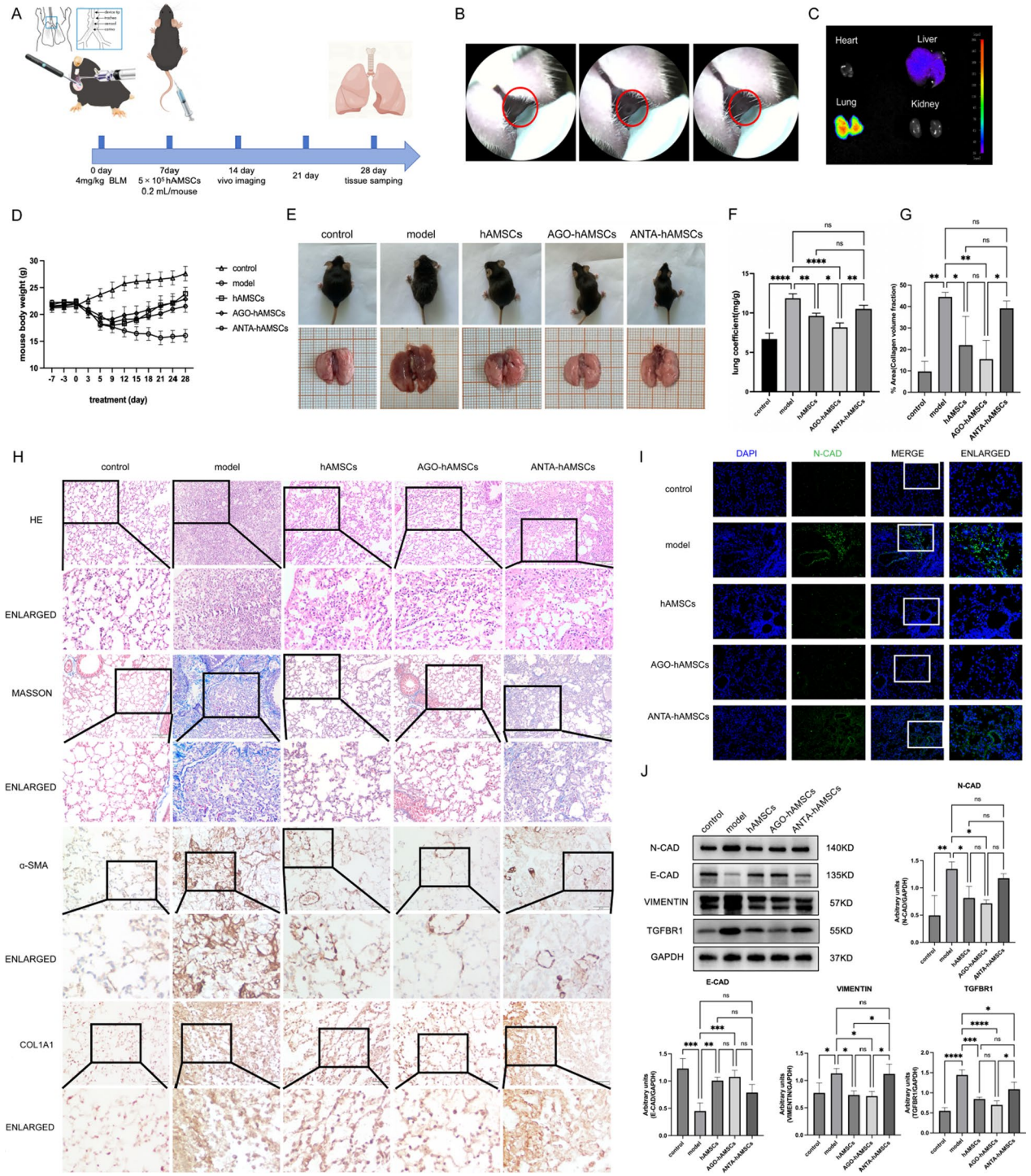

Fig. 3 Effects of hAMSCs with different hsa-miR181a-5p expression levels on lung fibrosis mice. **A** timeline of animal experiments. **B** Schematic diagram of the position of mouse modeling cannula. **C** In vivo imaging results of mice 7 days after injection of hAMSCs. **D** Changes in body weight of mice. **E** General condition and appearance of lung tissues of mice in each experimental group. **F** Lung index of mice after sampling. **G** %Area(collagen volume fraction):Percentage of positive area of collagen blue staining of mouse lung tissue sections using Masson staining. **H** HE and MASSON staining, expression of the Alpha-SMA marker, and the collagen marker COL1A1 in lung tissue sections from mice in each experimental group (scale = 50 μm or 100 μm). **I** N-CAD immunofluorescence staining results in lung tissue sections from mice in each experimental group (scale = 155.6 μm). **J** N-CAD, E-CAD, VIMENTIN, and TGFBR1 protein expression levels. Data are presented as the ($\bar{x} \pm s$, n = 4). ns: $P > 0.05$, *$P < 0.05$, **$P < 0.01$, ***$P < 0.001$, ****$P < 0.0001$

of mice in the model group continued to decrease, and those of mice in the stem cell treatment groups began to increase slowly. After 28 days, the body weights of mice in the control group remained stable, those of mice in the model group were gradually maintained, and those of mice in each stem cell treatment group continued to increase (Fig. 3D). Before sampling, mice in the control group were in a good mental state, had smooth fur, were agile, and breathed slowly; mice in the model group were depressed, had messy fur, dull hair, breathed rapidly, and were curled up with their backs arched; mice in the stem cell treatment groups had their mental state gradually recovered, their fur increased in luster, they were agile, and breathed rapidly; mice in the model group showed obvious congestion and swelling of lungs compared with the control group, and the congestion and swelling in the stem cell-treated groups showed various degrees of improvement (Fig. 3E). Comparing the lung indices of the mice(the lungs of the mice / the weight of the mice) (Fig. 3F), the lung indices of mice in the model group were significantly higher than those of mice in the control group ($P<0.0001$); the lung indices of mice in the hAMSCs and AGO-hAMSCs groups decreased to different degrees compared with those of mice in the model group ($P<0.05$, $P<0.01$), and those of mice in the ANTA-hAMSCs group showed a decreasing trend, although not significant, compared with those of mice in the model group.

For pathological structural changes (Fig. 3G, H), mice in the control group had a clear structural hierarchy of lung tissue, intact alveolar structure, normal arrangement of alveolar walls, and only a small portion of α-SMA and COL1A1 were expressed; mice in the model group had a collapsed alveolar structure, thickening of alveolar walls, obstruction of alveolar lumens, increase in lung tissue solidity, and obvious collagen deposition in the lung tissue, with a significantly higher collagen volume fraction than that in the control group ($P<0.01$); α-SMA and COL1A1 were expressed in large quantities; the lung tissues of all the stem cell treatment groups (hAMSCs, AGO-hAMSCs, and ANTA-hAMSCs groups) were partially restored, the solid changes in the lung tissues were reduced, and alveolar lumens were intact compared with those of the model group; however, the alveolar walls existed in different degrees of thickening. In the hAMSCs and AGO-hAMSCs groups, the recovery of the alveolar structure was more obvious, and the collagen volume fraction was significantly lower in the hAMSCs and AGO-hAMSCs group ($P<0.05$, $P<0.01$), there was no significant difference between the collagen volume fraction of the ANTA-hAMSCs group and that of the model group ($P>0.05$), or between the AGO-hAMSCs and hAMSCs groups ($P>0.05$), but the AGO-hAMSCs group collagen volume fraction was significantly lower than the ANTA-hAMSCs group ($P<0.01$), suggesting that the effect of the AGO-hAMSCs group was significantly better than that of the ANTA-hAMSCs group. α-SMA and COL1A1 expression were reduced to varying degrees in all stem cell treatment groups, with the reduction in α-SMA and COL1A1 expression being more pronounced in the hAMSCs and AGO-hAMSCs groups than the ANTA-hAMSCs group. These findings indicate that the mice in the model group had significant myofibroblast proliferation and collagen deposition, and the myofibroblast number and collagen deposition in the lung tissue of the mice in each stem cell treatment group were alleviated to a certain extent, with the hAMSCs and AGO-hAMSCs groups having a better therapeutic effect, and the ANTA-hAMSCs group having a poorer therapeutic effect.

The results of the EMT indices are illustrated in Fig. 3I, J. Mice in the model group showed a large loss of the epithelial cell marker E-CAD ($P<0.001$) and a significant increase in the protein expression levels of the mesenchymal cell markers N-CAD, VIMENTIN, and TGFBR1 ($P<0.05$ or $P<0.01$ or $P<0.0001$), compared with the control group. Compared with the model group, the hAMSCs group, the AGO-hAMSCs group E-CAD expression level was significantly restored ($P<0.01$ or $P<0.001$), the N-CAD, VIMENTIN, and TGFBR1 expression level was decreased ($P<0.05$ or $P<0.001$ or $P<0.0001$). E-CAD, N-CAD, and VIMENTIN protein expression in the ANTA-hAMSCs group showed a trend, although not significant, compared with the model group, and the TGFBR1 protein expression level was reduced ($P<0.05$). VIMENTIN protein expression in the hAMSCs and the AGO-hAMSCs groups was significantly reduced compared with that in the ANTA-hAMSCs group ($P<0.05$), and TGFBR1 protein expression in the AGO-hAMSCs group was significantly reduced compared with that in the ANTA-hAMSCs group ($P<0.05$). The above results showed that the lung tissue of mice in the model group showed obvious EMT, and the EMT of the lung tissue of mice in the hAMSCs and AGO-hAMSCs groups was significantly improved.The therapeutic effect of the ANTA-hAMSCs group was poor, and the degree of interstitialization of the lung tissue of the mice in the hAMSCs and AGO-hAMSCs groups was lower than that of the ANTA-hAMSCs group.

hAMSCs relieve fibrosis by promoting epithelial cell proliferation, reducing epithelial cell apoptosis, and attenuating epithelial mesenchymal transition through paracrine effects

Based on the fibrosis remission effects observed in animal studies, the cell experiments focused on the most critical

process in fibrosis: EMT. An in vitro EMT model of epithelial cells was established, and a transwell co-culture system was used to more accurately observe the effects of hAMSCs on EMT during fibrosis via paracrine effects. The EMT cell model was established first, and then the number and proportion of co-cultured cells were selected to observe the effects after co-culture.

The concentrations of TGFβ1 selected were 5 and 10 ng/mL, and the treatment duration was 24 and 48 h. After the cells were treated, the cells gradually changed from the typical characteristics of "paving-stone" state epithelial cells to the mesenchymal cell-like "long shuttle shape" (Fig. 4A). The expression of epithelial markers E-CAD and cytokeratin decreased ($P<0.05$, $P<0.01$, or $P<0.001$), and the expression of collagen production marker COL1A1 and mesenchymalization markers N-CAD, VIMENTIN, and ZO-1 increased ($P<0.05$, $P<0.01$, $P<0.001$, and $P<0.0001$) (Fig. 4B, C). Our experimental results confirmed that treatment with 5 ng/mL TGF-β1 for 24 h led to morphological changes in the cells, and both RT-qPCR and Western blot analyses of EMT-related markers demonstrated successful establishment of the epithelial-mesenchymal transition model. Additionally, at both 24 h and 48 h time points, there were no difference in the degree of mesenchymal transition between the 5 ng/mL and 10 ng/mL treatment groups, consistent with conclusions drawn from the literature. Further studies will involve co-culturing with amniotic mesenchymal stem cells for 48 h, taking care not to prolong the cell experiment duration to avoid affecting cell growth. Ultimately, we chose to treat A549 cells with 5 ng/mL TGF-β1 for 24 h.

Three cell co-culture hAMSCs:A549 ratios were selected: 1:1, 2:1, and 5:1. Morphological results showed that after the addition of hAMSCs co-culture, contrast with the model group, the morphology of A549 cells in the three co-culture groups (co-culture 1:1, co-culture 2:1, and co-culture 5:1) were mostly restored to the typical "paving-stone" state; however, no difference was observed in the morphology among the three co-culture groups(Fig. 4D). The epithelial marker E-CAD was significantly reduced in the model group compared with the control group ($P<0.0001$), COL1A1, N-CAD, and TGFBR1 expression was significantly increased ($P<0.0001$), and COL1A1, N-CAD, and TGFBR1 expression was decreased after the addition of hAMSCs co-culture ($P<0.05$, $P<0.01$, or $P<0.0001$); no difference among the three groups of co-culture groups was observed (Fig. 4E). This indicates that the mesenchymalization of cells after co-culture with hAMSCs was significantly higher than that in the control group. The degree of EMT could be alleviated after co-culture, but the alleviation effect showed no significant difference with the increase in the number of hAMSCs. In summary, the ratio 1:1 of the two cellular co-cultures was selected.

The timeline of the cell experiment after determining the drug concentration, treatment time, and the ratio of co-cultured cells is outlined in Fig. 4F. The cell morphology of each group was observed, and the morphological changes of mesenchymalization caused by TGFβ1 were improved after co-culture with hAMSCs. During the co-culture process, hAMSCs grew well in the Transwell chambers. Compared with the control group, the proportion of EdU and PCNA positive cells in the model group decreased ($P<0.05$, $P<0.01$) (Fig. 4G, H), indicating that the proportion of cells in the proliferative state decreased, whereas that of EdU and PCNA positive cells in the co-culture group significantly increased compared with the model group ($P<0.01$), and the proportion of cells in the proliferative state increased. This suggests that hAMSCs can improve TGFβ1 inhibition of epithelial cell proliferation. Compared with the control group, the proportions of total apoptotic cells and late apoptotic cells in the model group increased significantly ($P<0.01$) (Fig. 4I), and the proportions of total apoptotic cells and late apoptotic cells in the co-culture group were significantly lower than the model group ($P<0.01$). This indicates that hAMSCs could improve the apoptosis of epithelial cells caused

(See figure on next page.)

Fig. 4 hAMSCs ameliorate fibrosis by promoting epithelial cell proliferation, reducing epithelial cell apoptosis, and attenuating epithelial mesenchymal transition through paracrine effects. **A** Morphological changes of cells (scale bar = 100 μm). **B** Cellular epithelial mesenchymal transition, collagen production indices E-CAD, Cytokeratin, COL1A1, N-CAD, VIMENTIN, and ZO −1 mRNA expression levels. **C** N-CAD, E-CAD protein expression levels. **D** Morphological changes of cells after co-culture (scale bar = 100 μm). **E** mRNA expression levels of COL1A1, E-CAD, N-CAD, and TGFBR1, which are related to EMT. **F** Schematic illustration of the timeline of the cellular experiments with the morphology of A549 cells in the Transwells of the experimental groups. **F** Time axis of cell experiments and morphology of A549 cells and hAMSCs in Transwell (scale bar = 200 μm). **G** EdU staining and the proportion of EdU-positive cells (scale bar = 311.3 μm). **H** PCNA immunofluorescence staining and the proportion of PCNA-positive cells (scale bar = 311.3 μm). **I** Results of Annexin-FITC/PI staining and statistical graphs. **J** BAX immunofluorescence staining results (scale bar = 311.3 μm). **K** BAX mRNA expression level. **L** BAX protein expression level. **M** COL1A1 and N-CAD immunofluorescence staining results (scale bar = 311.3 μm). **N** COL1A1 and N-CAD mRNA expression level. **O** N-CAD protein expression level. **P** TGFBR1 mRNA expression level. **Q** TGFBR1 protein expression level. Data are presented as the ($\bar{x} \pm s$, n = 3). ns: $P>0.05$, *$P<0.05$, **$P<0.01$, ***$P<0.001$, ****$P<0.0001$

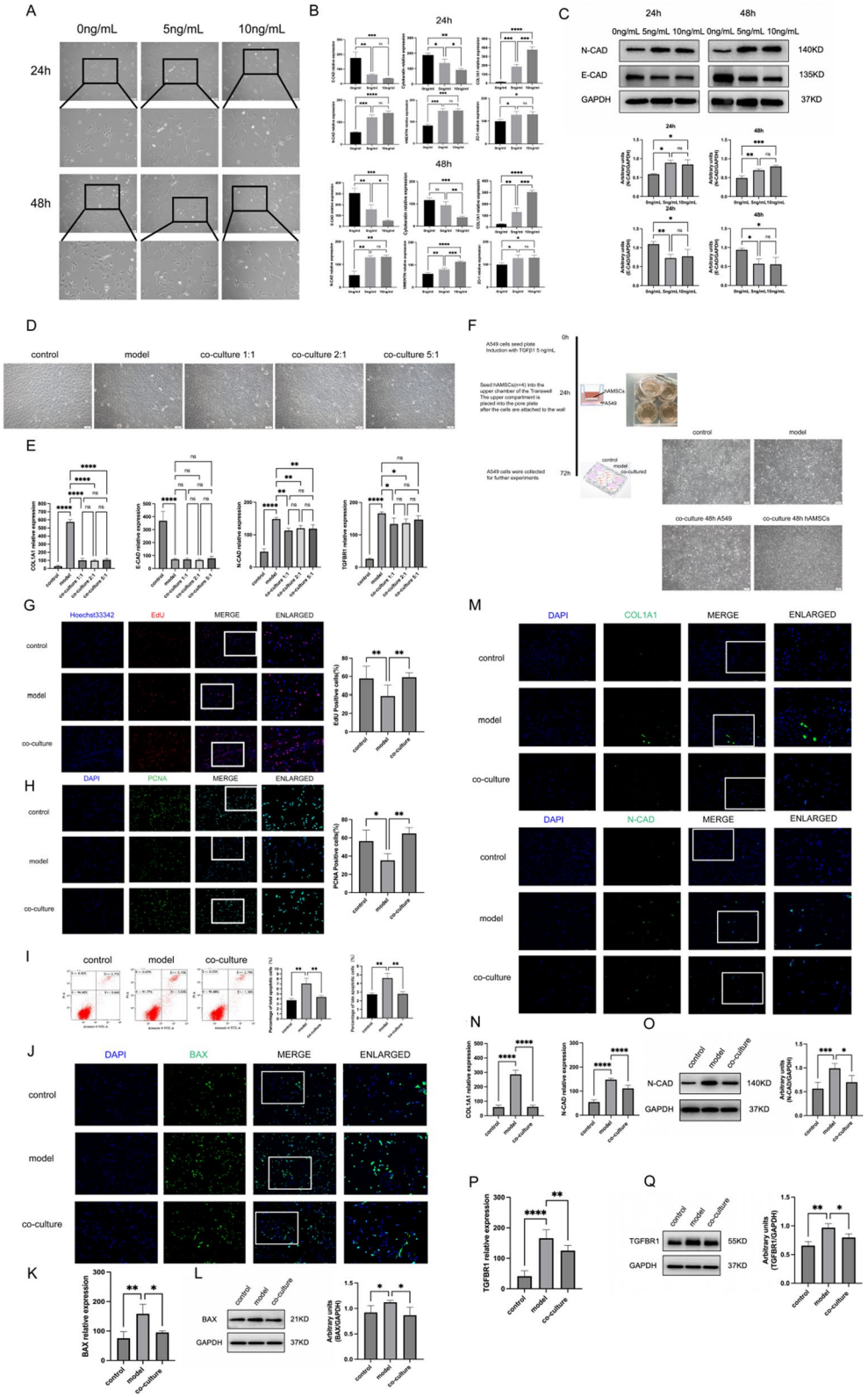

Fig. 4 (See legend on previous page.)

by TGFβ1. Compared with the control group, the expression levels of BAX mRNA and protein, a pro-apoptotic gene, were significantly increased in the model group ($P<0.05$, $P<0.01$) (Fig. 4J, K, L), whereas that of BAX in the co-culture group was significantly decreased compared with that in the model group ($P<0.05$). This suggests that co-culture with hAMSCs can reduce epithelial cell apoptosis by decreasing the expression of BAX, a pro-apoptotic gene. Compared with the control group, the expression levels of COL1A1 and N-CAD mRNA and protein in the model group were significantly increased ($P<0.001$ or $P<0.0001$) (Fig. 4M–O), and the expression levels of COL1A1 and N-CAD in the co-culture group were significantly decreased compared to those in the model group ($P<0.05$, $P<0.0001$). This indicates that co-culture with hAMSCs can reduce the collagen deposition and mesenchymalization of epithelial cells caused by TGFβ1. Compared with the control group, the cellular TGFBR1 mRNA and protein expression levels in the model group were significantly increased ($P<0.01$ or $P<0.0001$) (Fig. 4P, Q), whereas the cellular TGFBR1 expression in the co-culture group was decreased compared with that in the model group ($P<0.05$ or $P<0.01$). This indicates that cellular TGFBR1 expression increases under the effect of TGFβ1, and co-culture with hAMSCs can reduce the increase of cellular TGFBR1 expression caused by TGFβ1.

hAMSCs regulate mesenchymalization and cell cycle to retard fibrosis through hsa-miR-181a-5p/TGFBR1

The hAMSCs with different miR-181a-5p expression levels were co-cultured with A549 cell EMT model, as shown in Fig. 5A. The cell morphology results showed that the cells in the model group showed obvious "long shuttle" morphology compared with those in the control group. In the three groups of stem cell co-culture (hAMSCs co-culture, AGO-hAMSCs co-culture, ANTA-hAMSCs co-culture groups), most of the cells had typical "paving stone" state morphology, and there was no difference in the morphology of the cells among the three groups.

As shown in Fig. 5B, compared with the cells in the control group, FN1 and VIMENTIN levels were elevated in the model group ($P<0.01$, or $P<0.001$). Compared with the model group, FN1 and VIMENTIN were significantly reduced in the hAMSCs co-culture and AGO-hAMSCs co-culture groups ($P<0.05$ or $P<0.01$ or $P<0.001$) but did not statistically differ in the ANTA-hAMSCs co-culture group ($P>0.05$). FN1 was significantly lower in the AGO-hAMSCs co-culture group compared with the ANTA-hAMSCs co-culture group ($P<0.05$). These results indicate that the cells in the model group showed mesenchymalization, the hAMSCs co-culture group and AGO-hAMSCs co-culture group alleviated mesenchymalization significantly, and the degree of alleviation of mesenchymalization in the AGO-hAMSCs co-culture group was significantly better than that in the ANTA-hAMSCs co-culture group.

The TGFBR1 expression of the three stem cell co-culture groups is shown in Fig. 5C. The TGFBR1 expression of the AGO-hAMSCs co-culture group was significantly lower than that of the hAMSCs co-culture group ($P<0.05$); TGFBR1 expression was significantly increased in the ANTA-hAMSCs co-culture group compared with the hAMSCs co-culture group ($P<0.05$), there was a significant difference in TGFBR1 expression between the AGO-hAMSCs co-culture and ANTA-hAMSCs co-culture groups ($P<0.001$). These results confirmed the targeted association of hAMSCs with TGFBR1, a key gene in the fibrotic process, through the delivery of miR-181a-5p.

Given the observed effects, combined with the multi-targets pathways downstream of TGFβ1/TGFBR1, we next explored the underlying molecular mechanisms by DNBSEQ eukaryotic transcriptome resequencing. The samples were sent to Wuhan BGI for high-throughput DNBSEQ eukaryotic transcriptome resequencing. Quality control was performed according to the "RNA Sequencing Sample Quality Standards," assessing RNA concentration, RIN/RQN, and 28S/18S ratios. All samples met the quality standards and were classified as Class A. The original detection report is as follows: Data filtering was done using SOAPnuke (v1.5.6) on the raw data, resulting in clean data.Screening for differentially expressed transcriptome genes in the transcriptome analysis (Log_2(AGO-hAMSCs co-culture/hAMSCs co-culture) ≤ -1.5-fold changes) identified 15,626 differentially expressed genes, (Log_2(ANTA-hAMSCs co-culture/hAMSCs co-culture) ≥ 1.5-fold changes) differential genes had 17,118, and the two genomes intersected with 1,787 genes in the transcriptome. Based on the results of differentially expressed mRNAs, we performed KEGG enrichment analysis as shown in Fig. 5D.

Differential genes were enriched in the phosphatidylinositol signaling system, Inositol phosphate metabolism, Phospholipase D signaling pathway, Hippo signaling pathway, Regulation of actin cytoskeleton, Rap1 signaling pathway, TGF-beta signaling pathway, TNF signaling pathway, PI3K-Akt signaling pathway, p53 signaling pathway. Among them, Phosphatidylinositol signaling system, Inositol phosphate metabolism, Phospholipase D signaling pathway, PI3K-Akt signaling pathway, p53 signaling pathway are mainly involved in the regulation of cellular activities such as cell proliferation and survival, cell polarity and migration, and

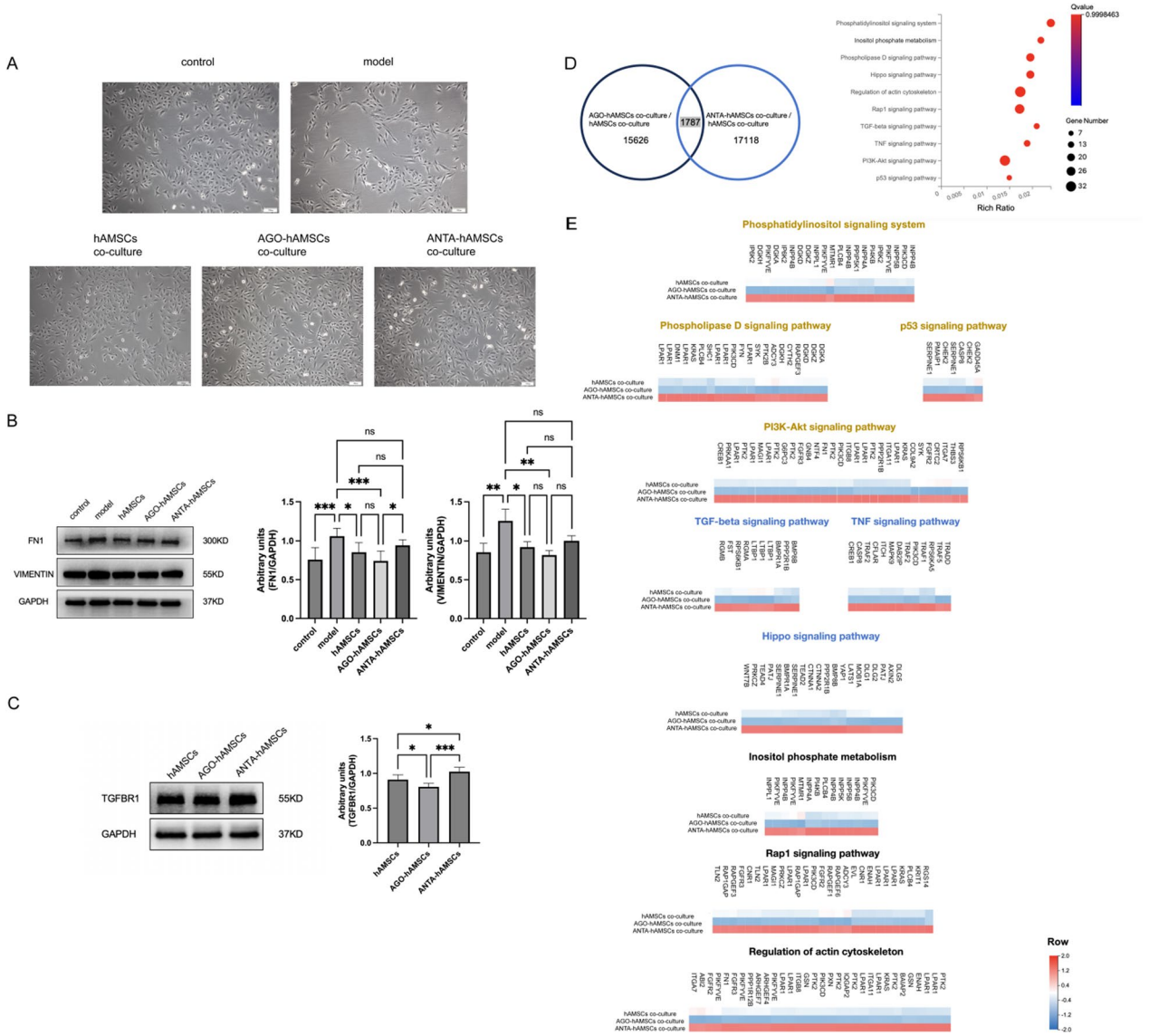

Fig. 5 hAMSCs regulate mesenchymal stromalization and cell cycle improvement of fibrosis through hsa-miR-181a-5p/TGFBR1. **A** Morphological results of co-cultured cells (scale bar = 100 μm). **B** Protein expression level of FN1 and VIMENTIN in each group. **C** Protein expression level of cellular TGFBR1. **D** Transcriptome results of VENN plots and KEGG pathway-enriched bubble plots; **E** KEGG-enriched gene sets of each pathway. Data are presented as the ($\bar{x} \pm s$, n = 3). ns: $P > 0.05$, *$P < 0.05$, **$P < 0.01$, ***$P < 0.001$

cell differentiation; Hippo signaling pathway, TGF-beta signaling pathway, TNF signaling pathway are mainly involved in the regulation of cellular activities such as cellular inflammation, fibrosis and other cellular activities. The specific gene sets of these pathways are shown in Fig. 5E. These results confirmed that hAMSCs are involved in the regulation of the cellular life cycle, cellular inflammation, and mesenchymalization through the delivery of miR-181a-5p to ameliorate fibrosis.

Discussion

The main findings of this study are: (1) hAMSCs exerted an anti-fibrotic effect and attenuated EMT both in vivo and in vitro. (2) hAMSCs ameliorated PF by promoting epithelial cell proliferation, reducing epithelial cell apoptosis, and attenuating EMT of epithelial cells through paracrine effects. (3) miR-181a-5p-overexpressed hAMSCs have a better therapeutic effect on the improvement of EMT in PF than miR-181a-5p-underexpressed hAMSCs. (4) hAMSCs regulate EMT in PF by delivering miR-181a-5p targeting TGFBR1.

The mechanism underlying the development of PF remains poorly understood, although it has been suggested that inflammatory responses, epithelial cell apoptosis, and EMT should be included. Therefore, alleviating the inflammatory response, improving epithelial cell apoptosis, alleviating the process of epithelial cell mesenchymalization, and promoting the neonatalization of type II alveolar epithelial cells are keys to treating PF. According to different etiologies, numerous existing modeling drugs and administration methods for PF have been developed [23, 56], among which BLM, paraquat, silica, lipopolysaccharide, carbon tetrachloride, and radiation are common. The modeling drug used in the present study was BLM, whose early alteration is the damage of epithelial cells, activation of inflammatory cells, promotion of inflammatory mediators release, and triggering the cellular inflammatory response, alveolar macrophages, and other activated cells release fibrosis-associated cytokines and growth factors, such as TGF-β1. In the subacute stage, fibroblast proliferation with EMT occurs in the lung tissues, ultimately leading to fibrotic matrix deposition [56]. These mechanisms are mostly similar to the existing triggers in patients with PF. The cellular experimental modeling drug selection of TGF-β1-induced A549 cells as a model of EMT in PF, an in vitro EMT model [57], is important for studying EMT as a process in the fibrosis process.

Most of the existing studies have demonstrated that after infusion of MSCs into fibrotic mice, the cells homed in the injured lung tissues of mice for tissue repair and regeneration [58, 59]. MSCs from different sources have shown clear therapeutic effects on PF through their anti-apoptotic, anti-inflammatory, and anti-oxidative stress effects [60]. Our results showed that hAMSCs alleviated interstitial deposition and fibrosis in the mouse lung tissue by inhibiting EMT. It has been demonstrated that paracrine secretion is the main mechanism by which MSCs play a role in tissue repair and regeneration [61], and the Transwell co-culture method used in this study demonstrated that MSCs act through paracrine secretion. hAMSCs not only act through paracrine secretion but also differentiate into specific types of cells and directly replace defective cells in damaged tissues or organs. For example, hematopoietic stem cells can differentiate into specific cell types and replace defective cells in damaged tissues or organs. Hematopoietic stem cells can differentiate into different types of blood cells to treat blood disorders [62, 63], and neural stem cells can differentiate into neurons to repair neurological damage [64].

In this study, the relative expression of miR-181a-5p in the lung tissues of mice with PF was significantly lower than that in normal mice but was highly expressed in normal human lung tissues and stem cells. Database prediction of hsa-miR-181a-5p intersecting target genes revealed that it was concentrated in the key immune activation and inflammatory pathway of PF TGFβ signaling pathway, MAPK, PI3K- AKT, and RAS signaling pathways involved in vasoconstriction, inflammation, and fibrosis. These results suggest that miR-181a-5p plays an important role in inhibiting PF. When hAMSCs with different miR-181a-5p expression levels were co-cultured with a cellular EMT model and the related changes were detected, the degree of mitigation of mesenchymal stromalization in the AGO-hAMSCs co-culture group was significantly better than that in the ANTA-hAMSCs co-culture group, indicating that miR-181a-5p delivered by hAMSCs plays a key role in the improvement of EMT. In this study, the body weight, general status, lung index, and lung appearance of mice collectively showed that to alleviate the degree of fibrosis, the hAMSCs and AGO-hAMSCs groups were more effective than the ANTA-hAMSCs group, suggesting that miR-181a-5p plays an important role in the treatment of PF with hAMSCs. Based on the observation of EMT-related proteins, the lung tissue of mice in the model group showed obvious EMT. hAMSCs alleviated mesenchymal deposition and fibrosis by improving EMT, and miR-181a-5p delivered by hAMSCs played an important role in improving EMT. Taken together, these results suggest that hAMSCs inhibit fibrosis progression by delivering miR-181a-5p to alleviate EMT. The ameliorative effect of miR-181a-5p on EMT has also been demonstrated in cancer, and the overexpression of miR-181a-5p in non-small-cell lung cancer (NSCLC) inhibits the NF-κB pathway through the targeting of GTSE1 and activation of the p53 pathway. NF-κB pathway inhibits NSCLC cell proliferation, migration, and EMT [65]. In papillary thyroid carcinoma (PTC), miR-181a-5p promotes cell growth, migration, and EMT by downregulating KLF15 [66].

For the EMT model of TGFβ1-treated cells, hAMSCs could attenuate collagen deposition and EMT. TGF-β1 treatment of HK-2 cells induces EMT, inhibits HK-2 cell proliferation, and promotes apoptosis. Still, when co-cultured with MSCs, EMT is alleviated, proliferation is promoted, and apoptosis is slowed, consistent with our findings [67].

The results of dual luciferase reporter showed that miR-181a-5p could bind to TGFBR1 in a targeted manner, TGFβ1 increased cellular TGFBR1 expression, and co-culturing with hAMSCs decreased cellular TGFBR1 expression. TGFBR1 in the AGO-hAMSCs co-culture and hAMSCs co-culture groups was significantly lower than in the ANTA-hAMSCs co-culture group, suggesting that hAMSCs target TGFBR1 by delivering miR-181a-5p. Transcriptome results showed that the Hippo signaling

pathway, TGF-beta signaling pathway, and TNF signaling pathway are mainly involved in the regulation of cellular inflammation, fibroblasts, and fibrosis. Therefore, it is speculated that hAMSCs regulate the intermediate stromalization of the fibrotic process through the miR-181a-5p/TGFBR1/TGF-beta signaling pathway, which warrants further studies.

AT2 is involved in physiological alveolar cell composition and differentiation, lung immunity and defense, lung injury repair, and maintenance of alveolar surfactants [68]. MSCs can directly colonize and differentiate into AT2 during lung tissue repair, providing an important basis for MSCs to promote lung injury repair and participate in tissue reconstruction [69]. In the in vitro model, hAMSCs ameliorated TGFβ1-induced inhibition of epithelial cell proliferation and improved apoptosis by decreasing the expression of pro-apoptotic gene BAX. Based on the transcriptome sequencing results, the phosphatidylinositol signaling system, inositol phosphate metabolism, Phospholipase D signaling pathway, PI3K-Akt signaling pathway, p53 signaling pathway, and PI3K-Akt signaling pathway were involved in differential gene enrichment. PI3K-Akt and p53 signaling pathways are mainly involved in regulating cellular activities, such as cell proliferation and survival, cell polarity and migration, and cell differentiation. The PI signaling system can regulate the cellular activities of MSCs by activating a series of enzymes, such as PI3K, Akt, and ERK, and PI3K-AKT is involved in the regulation of MSCs. PI3K -AKT is involved in regulating the proliferation and differentiation of MSCs and enhancing the immunosuppressive effect of MSCs [70, 71]. miR-181a-5p is involved in regulating cell proliferation through the modulation of the PI3K-AKT pathway [72]. However, whether the delivery of miR-181a-5p by hAMSCs is involved in the regulation of cell proliferation via the PI3K-AKT pathway remains to be determined.

In recent years, significant progress has been made in the study of signaling pathways involved in the development of fibrosis. Emerging research indicates that these pathways can be targeted by stem cells to alleviate various fibrotic diseases. Below is an overview of some key signaling pathways critical to the progression of fibrosis: (1) TGF-β Signaling Pathway: Transforming growth factor-beta (TGF-β) is a major cytokine in the processes of fibrosis and inflammation. It primarily regulates inflammatory responses, EMT, extracellular matrix (ECM) production, and fibroblast activation and proliferation through the activation of Smad proteins. Targeted therapies for fibrosis can be developed using TGF-β-related antibodies and small molecule inhibitors [73, 74]. (2)MAPK Signaling Pathway: The MAPK family, which includes p38 MAPK, ERK, and JNK, plays a crucial role in the development of fibrosis by regulating cell proliferation, survival, migration, and the production of pro-fibrotic mediators. In fibrosis progression, the p38 pathway is associated with cellular stress, inflammation, and apoptosis; its activation promotes the production of inflammatory factors and alters fibroblast functionality. ERK activation enhances fibroblast proliferation and collagen synthesis, while JNK activation increases the expression of inflammatory factors, exacerbating the fibrotic process [75, 76]. (3)PI3K/AKT Signaling Pathway: The PI3K/AKT pathway is involved in the regulation of oxidative stress, autophagy, inflammatory responses, and cell proliferation and survival, all of which contribute to the development of fibrosis [77]. For instance, activation of the PI3K/AKT pathway can promote autophagy and alleviate oxidative stress, thereby protecting against renal fibrosis. In liver fibrosis, this pathway's activation promotes the proliferation of hepatic stellate cells (HSCs) and ECM synthesis, worsening liver fibrosis. Additionally, the PI3K/AKT pathway exhibits anti-apoptotic effects, aiding fibroblast survival and continued ECM production in damaged tissues [78]. (4)mTOR Signaling Pathway: The mTOR pathway plays a pivotal role in cell growth, metabolism, proliferation, survival, and autophagy. Research has demonstrated that mTOR expression in the lungs of patients with idiopathic pulmonary fibrosis correlates closely with fibrosis scores and declines in lung function [79]. Abnormal activation of mTOR is linked to damage and repair dysregulation in alveolar epithelial cells. Inhibiting mTOR signaling can slow the progression of liver fibrosis by suppressing the activation and proliferation of HSCs, as well as reducing ECM secretion. Furthermore, mTOR activation can promote the transformation of renal tubular epithelial cells into mesenchymal cells, leading to fibrosis [80, 81]. (5)Wnt/β-Catenin Signaling Pathway: The Wnt/β-catenin pathway regulates cell proliferation and differentiation by influencing the expression of cyclin and matrix metalloproteinase (MMP) genes. This pathway facilitates the migration and accumulation of fibroblasts at damaged sites, thereby contributing to the development of pulmonary fibrosis [82].These signaling pathways do not operate in isolation; they interact and coordinate with each other in the progression of lung fibrosis. As our understanding of these fibrotic signaling pathways deepens, more targeted therapeutic approaches may emerge. The potential of stem cell therapy for fibrotic diseases is immense, yet further research is necessary to elucidate the molecular mechanisms by which stem cells regulate the fibrotic process and to develop new strategies to enhance their anti-fibrotic effects.

The primary mechanisms of stem cell therapy for fibrosis include: (1)Anti-inflammatory Effects: Stem cells secrete anti-inflammatory cytokines, such as IL-10 and

PGE2, which inhibit inflammatory responses and reduce the infiltration of inflammatory cells during the fibrotic process. This anti-inflammatory action not only alleviates local tissue damage but also creates a more favorable microenvironment for subsequent repair processes [83]. (2)Immune Regulation: Stem cells can modulate the activity of natural killer cells, T cells, and B cells, thereby reducing autoimmune responses and slowing the progression of fibrosis. By regulating the immune system, stem cells can decrease the risk of fibrosis associated with autoimmune diseases [83, 84]. (3)Promotion of Tissue Repair: Stem cells have the ability to differentiate into cell types specific to damaged tissues, such as alveolar epithelial cells and hepatocytes, thus facilitating the reconstruction of tissue structure and function. This regenerative capacity is crucial for restoring normal tissue function, especially in cases of severe damage [85]. (4)Inhibition of Myofibroblast Activation: Stem cells secrete factors that inhibit the activation and proliferation of myofibroblasts, reducing the deposition of ECM. By modulating the activity of myofibroblasts, stem cells help control the progression of fibrosis [86]. (5)Promotion of Extracellular Matrix Degradation: Stem cells can enhance the expression of MMPs, thereby facilitating ECM degradation and alleviating fibrosis. This mechanism is essential for maintaining the normal structure and function of tissues [87]. (6)Antioxidant Effects: Stem cells possess antioxidant properties that enable them to scavenge reactive oxygen species (ROS), mitigating oxidative stress and protecting alveolar epithelial cells. By reducing oxidative stress, stem cells not only protect cells but also promote their survival and functional recovery [88]. (7)Paracrine Effects: Stem cells secrete various growth factors and cytokines, such as hepatocyte growth factor (HGF), angiopoietin-1, and vascular endothelial growth factor (VEGF), through paracrine signaling. These factors promote angiogenesis, alleviate inflammation and fibrosis, and facilitate tissue regeneration and repair [89, 90].

With the recent advancements in emerging technologies, researchers have begun to explore the effects of preconditioned stem cell therapies for pulmonary fibrosis, building on previous studies focused solely on the efficacy of stem cells. The following are some key approaches being investigated: (1)Nano-engineered Stem Cells: Stem cells engineered using nanotechnology can enhance their antioxidant and anti-fibrotic capabilities, prolong their survival in vivo, and allow for real-time visualization of therapeutic effects. This application improves the precision and effectiveness of stem cell therapies [69, 91]. (2) Gene-modified Stem Cells: By employing genetic engineering techniques to introduce anti-fibrotic genes into stem cells, their therapeutic effectiveness can be significantly enhanced. This method enables targeted intervention tailored to specific pathological mechanisms [92]. (3)Combination of Stem Cells with Clinical Drug Treatments: This approach has shown superior efficacy compared to either treatment alone, providing theoretical support for the clinical translation of stem cells. Mesenchymal stem cells can serve as carriers for delivering other bioactive substances, such as genes, drugs, or therapeutic proteins. This combination strategy holds promise for achieving more precise treatment outcomes and improving the survival rates and quality of life for patients with pulmonary fibrosis [93, 94].

These strategies can be used individually or in combination to enhance the effectiveness of stem cell therapies for fibrosis. As research progresses, the mechanisms underlying stem cell treatment for fibrosis will become clearer, offering more strategies and methods for clinical application. Integrating basic research with clinical practice is expected to improve the prognosis for fibrosis patients and advance the application of stem cell therapies in fibrosis management.

Currently, the challenges faced by MSCs transplantation include:(1)Immune Rejection: Due to their inherent immunogenic properties, MSCs may trigger an immune response in the host after transplantation, leading to immune rejection [95, 96]. (2)Safety Concerns: The long-term safety and potential tumorigenicity of MSCs require further evaluation. Animal studies and clinical research have demonstrated that the introduction of stem cells into animals and humans can cause varying degrees of vascular embolism, and even result in mortality. There is a risk that MSCs transplantation could lead to tumor growth within the body [96, 97]. (3) Dynamic Changes: While emerging technologies such as single-cell sequencing have provided some insights [98], research on the dynamic changes occurring with MSCs during the fibrotic process remains limited. (4)Lack of Standardized Treatment Protocols: Studies have indicated that variations in stem cell donors, transplantation dosage, and timing can all influence efficacy [99–101], leading to limited comparability and reproducibility of research results. Further investigation is needed to determine the optimal sources, donor conditions, culture conditions, routes of administration, dosages, and intervals for MSCs and MSC-derived extracellular vesicles (EVs) to enhance therapeutic effects and improve the design of clinical intervention trials, ensuring the safety and evidence-based nature of MSCs therapies. Specific and effective administration methods should be selected based on experimental protocols or patient disease characteristics.To address the existing challenges in MSCs therapy for pulmonary fibrosis, the following measures can be implemented: (1)Enhance Basic Research: Investigating the mechanisms of disease, treatment processes,

and intercellular communication can provide more reliable scientific foundations for future clinical research and applications. (2)Support with Clinical Data: Further clinical studies are essential, requiring a systematic collection of extensive clinical trial data to evaluate the long-term efficacy and safety of MSCs therapy for pulmonary fibrosis, thus promoting the clinical application of these treatments. Additionally, long-term follow-up studies can help assess the durability of treatment effects and potential adverse impacts.

In summary, the treatment of pulmonary fibrosis with mesenchymal stem cells and their extracellular vesicles has made significant strides after years of research. This is especially pertinent given the rising incidence of pulmonary fibrosis related to COVID-19. With the collaborative efforts of researchers and healthcare professionals, further exploration of the relevant details will likely lead to the widespread clinical application of MSCs and their extracellular vesicles in treating various diseases.

Conclusions

This study reveals for the first time that the therapeutic effect of early intervention of hAMSCs delivering miR-181a-5p on PF and highlights the effect of hAMSCs on common causes of PF by taking lung tissue injury, alveolar epithelial cell changes, epithelial cell proliferation and apoptosis, and changes in EMT as the starting points. hAMSCs safeguard PF by targeting TGFBR1 through the delivery of miR-181a-5p (Fig. 6). Our findings provide a basis for the basic research on the early intervention of hAMSCs in the clinical treatment of PF, at the same time provide a new idea for the development of hAMSCs biomedical products and technologies.

Main reagents

Name	Manufacturer
Stem cell lipid differentiation medium	Cyagen HUXXC-90031
Stem cell osteogenic differentiation medium	Cyagen HUXXC-90021
Stem cell flow phenotypic identification kit	BD 562245
DMEM/F12	Gibco C11330500BT
FBS	Gibco A5669701
P/S	Gibco 15,640,055
miRNA agomir, miRNA antagomir	Suzhou Genepharma Co.,Ltd
OPTI-MEM	GIBCO 31985070
LIPO-2000	Solarbio L7800
TRIzol reagent	Invitrogen
RNA isolation kit	Qiagen
Primer, miRNA reverse transcription kit, miRNA fluorescence quantitative PCR kit	Sangon
PrimeScript™ RT reagent Kit (Perfect Real Time)	Takara RR037A
TB Green® Premix Ex Taq™(Tli RNaseH Plus)	Takara RR420A

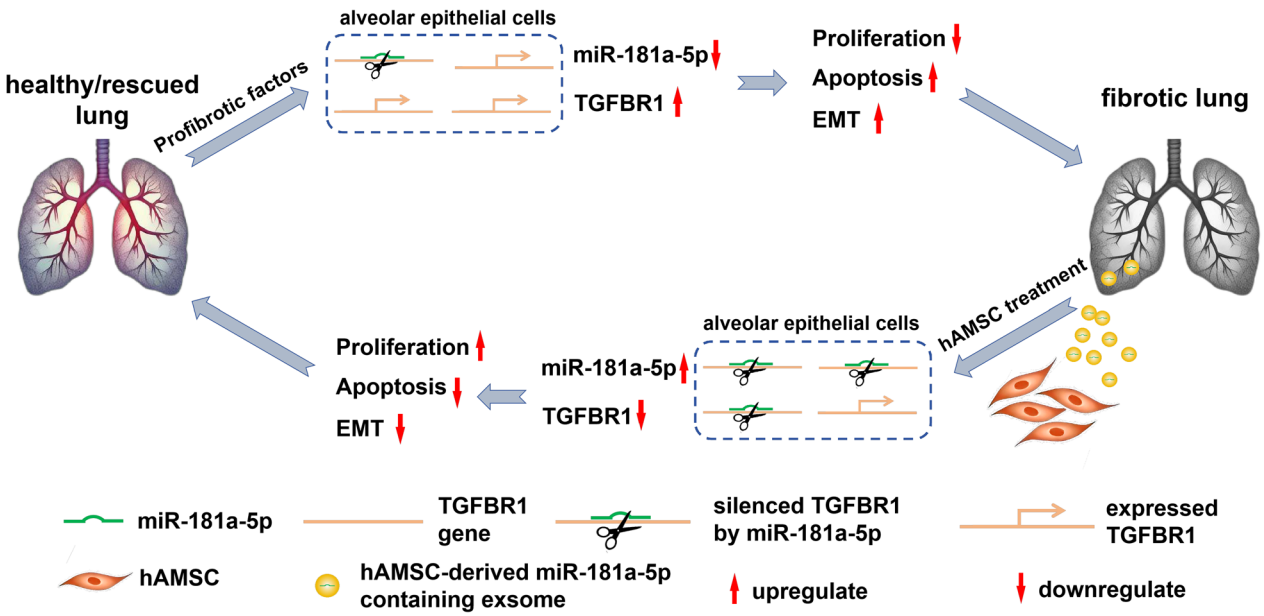

Fig. 6 Article summary drawing

Name	Manufacturer
BLM	MCE HY-17565
α-Smooth Muscle Actin(D4K9N) XP® Rabbit mAb	Cell Signaling TECHNOLOGY #19,245
Vimentin(D21H3)XP® Rabbit mAb	Cell Signaling TECHNOLOGY #5741
PCNA Antibody(PC10)	SANTA sc-56
Anti-Fibronectin Antibody	abcam ab268020
GAPDH(14C10)Rabbit mAb	Cell Signaling TECHNOLOGY #2118
E-Cadherin(24E10)Rabbit mAb	Cell Signaling TECHNOLOGY #3195
Anti-Collagen Type I/COL1A1 Antibody	BOSTER BA0325
N-Cadherin (D4R1H) XP® Rabbit mAb	Cell Signaling TECHNOLOGY #13,116
Anti-TGF beta Receptor I	abcam ab235578
BAX Polyclonal antibody	proteintech 50,599–2-Ig
TGFβ1	MCE HY-P7118
PKH-26	sigma-aldrich PKH26GL
YF® Dye/Rhodamine Phalloidin Conjugates	UE YP0059S
EdU Dyeing kit	RIBOBIO C10310-1
Annexin V-FITC/PI Cell apoptosis detection kit	YEASEN 40302ES50

Main instruments and consumables

Name	Manufacturer
Micropipette	Eppendorf
Flow cytometer	USA Becton Dickinson FACSAriaII
Ice machine	JPN SANYO SIM-F124
Gel imaging system	USA Bio-Rad ChemiDoc touch
Water purification apparatus	USA MILLI-Q
Refrigerated centrifuge	GER EPPENDORF Centrifuge 5804R
Inverted phase contrast microscope	JPN Olympus IX-71-S8F
Fluorescence microscope	Leica DMi8
Microplate reader	AUS Tecan Tecan Safire
Electronic scales	GER Sartorius BP121S
Automatic high-pressure disinfection cabinet	CHN MMM-group Ecocell
CO_2 incubator	ThermoForma 3141-I/R
−80°C ultra cold storage freezer	CHN Haier DW-86L486
Cell culture bottle	USA CORNING 25cm^2/75cm^2
24-well round cell crawl	WHB WHB-24-CS
TRANSWELL Co-culture plate	BIOFIL TCS016006
Endotracheal microsyringe	Shanghai Yuyan Instruments Co.,Ltd. YAN 30012
Visual ear harvester	Xiaomi Technology Co., Ltd Bebird R1

Abbreviations

AT2	Alveolar epithelial type II cells
α-SMA	α-Smooth muscle actin
BAX	BCL2-associated X protein
BCA	Bicinchoninic acid assay
BLM	Bleomycin
CCK-8	Cell counting Kit-8
cDNA	Complementary deoxyribonucleic acid
COL1A1	Collagen type I alpha 1 chain
ECL	Enhanced chemiluminescence
E-CAD	E-cadherin
EdU	5-Ethynyl-2′- deoxyuridine
EMT	Epithelial-mesenchymal transition
FBS	Fetal Bovine Serum
FITC	Fluorescein isothiocyanate isomer I
FN1	Fibronectin-1
GAPDH	Glyceraldehyde-3-phosphate dehydrogenase
hAMSCs	Human Amniotic Mesenchymal Stem Cells
N-CAD	N-cadherin
NSCLC	Non-small-cell lung cancer
PBS	Phosphate-Buffered Saline
PCNA	Proliferating cell nuclear antigen
PF	Pulmonary fibrosis
PI	Propidium iodide
RIPA	RIPA Lysis Buffer
RNA	Ribonucleic acid
P/S	Penicillin-streptomycin
RT-qPCR	Reverse transcription-quantitative realtime PCR
SDS	Sodium dodecyl sulfate
SPC	Surfactant protein C
TBS	Tris Buffered Saline
TGFβ1	Transforming growth factor beta 1
TGFBR1	Transforming growth factor beta receptor 1
WB	Western blotting
ZO-1	Zonula occludens-1

Supplementary Information

The online version contains supplementary material available at https://doi.org/10.1186/s13287-024-04095-3.

Additional file 1.

Acknowledgements
The work was supported by the Key Laboratory of Cell Engineering of Guizhou Province. The authors declare that they have not use AI-generated work in this manuscript in this section. We would like to thank Editage for providing English language editorial assistance.

Author contributions
YW and CL contributed to the experiment, data collection, data analysis, and manuscript writing. YZ, NW and GJ contributed to the manuscript writing and editing. HY, DW, HW, ZF and CL contributed to the animal experiment and cell experiment. SX, LY and ZH contributed to the project design and development, data collection, analysis, manuscript writing and editing, and final approval of the manuscript. All authors read and approved the final manuscript.

Funding
This work is financially supported by National Natural Science Foundation of China (No: 32270848), Guizhou Province Science and Technology Project (Qian Ke He [2020] 4Y192), Collaborative Innovation Center of Chinese Ministry of Education(Grant Number:2020–39), Science and Technology Foundation of Guizhou (No. QKH-JC-ZK[2023]YB586) and Guizhou Province High Level Innovative Talent Training Program-"1000"Talents (to N.W.).

Availability of data and materials
Data and materials used and/or analysed during the current study are available from the corresponding author on reasonable request.The databases used in the article are presented in Methods.The sequencing data supporting the results presented in this study are deposited in Additional file 1.

Declarations

Ethics approval and consent to participate

Animals were treated in accordance with the Basel Declaration in the context of phase experimental animals. Human material have been performed in accordance with the Declaration of Helsinki, informed consent was obtained from volunteers before sample collection. (1) Title of the approved project: This study is a part of National Natural Science Foundation of China (No: 32270848): Human amniotic mesenchymal stem cell delivery of miR-181a dual-targeted silencing of TNF-α/TGFBR and SRCIN1 for early intervention in pulmonary fibrosis. (2) Name of the institutional approval committee or unit: This study was approved by the Laboratory Animal Welfare AND Ethics Committee of Zunyi Medical University (Approval number: Appl. No. ZMU22-2203–022, Date of approval:2022.03.17) and the Ethics Committee of Zunyi Medical University (Approval number: (2022) 1–142, Date of approval:2022.03.17).

Competing interests

The authors declare no conflict of interest.

Author details

[1]Key Laboratory of Cell Engineering of Guizhou Province, Affiliated Hospital of Zunyi Medical University, Zunyi 563000, Guizhou, China. [2]Collaborative Innovation Center of Chinese Ministry of Education, Zunyi Medical University, Zunyi 563003, Guizhou, China. [3]Department of Prevention Healthcare, Southwest Hospital, First Affiliated Hospital of the Army Medical University, Chongqing 400038, China. [4]Department of Cardiothoracic Surgery, Liuzhou People's Hospital, Liuzhou 545001, Guangxi, China. [5]Key Laboratory of Basic Pharmacology of Ministry of Education and Joint International Research Laboratory of Ethnomedicine of Ministry of Education, Zunyi 563000, Guizhou, China. [6]Department of Pediatrics, Affiliated Hospital of Zunyi Medical University, Zunyi 563000, Guizhou, China. [7]Center of Tissue Engineering and Stem Cell Research, Guizhou Medical University, Guiyang 550025, Guizhou, China. [8]Department of Pediatric Hematology, The Affiliated Hospital of Guizhou Medical University, Guiyang 550025, Guizhou, China.

Received: 11 September 2024 Accepted: 4 December 2024
Published online: 05 January 2025

References

1. Kalchiem-Dekel O, Galvin JR, Burke AP, et al. Interstitial lung disease and pulmonary fibrosis: a practical approach for general medicine physicians with focus on the medical history. J Clin Med. 2018. https://doi.org/10.3390/jcm7120476.
2. Raghu G, Collard HR, Egan JJ, et al. An official ats/ers/jrs/alat statement: Idiopathic pulmonary fibrosis: evidence-based guidelines for diagnosis and management. Am J Respir Crit Care Med. 2011;183(6):788–824. https://doi.org/10.1164/rccm.2009-040GL.
3. Huang WJ, Tang XX. Virus infection induced pulmonary fibrosis. J Transl Med. 2021;19(1):496. https://doi.org/10.1186/s12967-021-03159-9.
4. Wang YY, Zhang CY, Ma YQ, et al. Therapeutic effects of c-28 methyl ester of 2-cyano-3,12-dioxoolean-1,9-dien-28-oic acid (cddo-me; bardoxolone methyl) on radiation-induced lung inflammation and fibrosis in mice. Drug Des Devel Ther. 2015;9:3163–78. https://doi.org/10.2147/dddt.S80958.
5. Rivera-Ortega P, Hayton C, Blaikley J, et al. Nintedanib in the management of idiopathic pulmonary fibrosis: Clinical trial evidence and real-world experience. Ther Adv Respir Dis. 2018;12:1753466618800618. https://doi.org/10.1177/1753466618800618.
6. George PM, Wells AU. Pirfenidone for the treatment of idiopathic pulmonary fibrosis. Expert Rev Clin Pharmacol. 2017;10(5):483–91. https://doi.org/10.1080/17512433.2017.1295846.
7. Bazdyrev E, Rusina P, Panova M, et al. Lung fibrosis after covid-19: Treatment prospects. Pharmaceuticals (Basel). 2021. https://doi.org/10.3390/ph14080807.
8. Meyer KC. Pulmonary fibrosis, part i: epidemiology, pathogenesis, and diagnosis. Expert Rev Respir Med. 2017;11(5):343–59. https://doi.org/10.1080/17476348.2017.1312346.
9. Perez-Favila A, Garza-Veloz I, Hernandez-Marquez LDS, et al. Antifibrotic drugs against idiopathic pulmonary fibrosis and pulmonary fibrosis induced by covid-19: Therapeutic approaches and potential diagnostic biomarkers. Int J Mol Sci. 2024. https://doi.org/10.3390/ijms25031562.
10. Yoon H, Dean LS, Jiyarom B, et al. Single-cell rna sequencing reveals characteristics of myeloid cells in post-acute sequelae of sars-cov-2 patients with persistent respiratory symptoms. Front Immunol. 2023;14:1268510. https://doi.org/10.3389/fimmu.2023.1268510.
11. Patrucco F, Solidoro P, Gavelli F, et al. Idiopathic pulmonary fibrosis and post-covid-19 lung fibrosis: links and risks. Microorganisms. 2023. https://doi.org/10.3390/microorganisms11040895.
12. Adams TS, Schupp JC, Poli S, et al. Single-cell rna-seq reveals ectopic and aberrant lung-resident cell populations in idiopathic pulmonary fibrosis. Sci Adv. 2020;6(28):eaba 983. https://doi.org/10.1126/sciadv.aba1983.
13. Park SJ, Hahn HJ, Oh SR, et al. Theophylline attenuates BLM-induced pulmonary fibrosis by inhibiting th17 differentiation. Int J Mol Sci. 2023. https://doi.org/10.3390/ijms24021019.
14. McElroy AN, Invernizzi R, Laskowska JW, et al. Candidate role for toll-like receptor 3 l412f polymorphism and infection in acute exacerbation of idiopathic pulmonary fibrosis. Am J Respir Crit Care Med. 2022;205(5):550–62. https://doi.org/10.1164/rccm.202010-3880OC.
15. Tsukui T, Sun KH, Wetter JB, et al. Collagen-producing lung cell atlas identifies multiple subsets with distinct localization and relevance to fibrosis. Nat Commun. 2020;11(1):1920. https://doi.org/10.1038/s41467-020-15647-5.
16. Parimon T, Yao C, Stripp BR, et al. Alveolar epithelial type ii cells as drivers of lung fibrosis in idiopathic pulmonary fibrosis. Int J Mol Sci. 2020. https://doi.org/10.3390/ijms21072269.
17. Tran S, Ksajikian A, Overbey J, et al. Pathophysiology of pulmonary fibrosis in the context of covid-19 and implications for treatment: a narrative review. Cells. 2022. https://doi.org/10.3390/cells11162489.
18. Chilosi M, Caliò A, Rossi A, et al. Epithelial to mesenchymal transition-related proteins zeb1, β-catenin, and β-tubulin-iii in idiopathic pulmonary fibrosis. Mod Pathol. 2017;30(1):26–38. https://doi.org/10.1038/modpathol.2016.147.
19. Zeng M, Feng A, Ren Y, et al. Salvia miltiorrhiza bunge extract and przewalskin ameliorate bleomycin-induced pulmonary fibrosis by inhibition of apoptosis, oxidative stress and collagen deposition via the tgf-β1 pathway. Phytomedicine. 2024;125: 155339. https://doi.org/10.1016/j.phymed.2024.155339.
20. Lee H, Jeong OY, Park HJ, et al. Promising therapeutic effects of embryonic stem cells-origin mesenchymal stem cells in experimental pulmonary fibrosis models: Immunomodulatory and anti-apoptotic mechanisms. Immune Netw. 2023;23(6):e45. https://doi.org/10.4110/in.2023.23.e45.
21. Amano H, Matsui Y, Hatanaka K, et al. Vegfr1-tyrosine kinase signaling in pulmonary fibrosis. Inflamm Regen. 2021;41(1):16. https://doi.org/10.1186/s41232-021-00166-7.
22. Margaritopoulos GA, Antoniou KM, Karagiannis K, et al. Investigation of angiogenetic axis angiopoietin-1 and -2/tie-2 in fibrotic lung diseases: A bronchoalveolar lavage study. Int J Mol Med. 2010;26(6):919–23. https://doi.org/10.3892/ijmm_00000543.
23. Moodley Y. Contemporary concise review 2023: interstitial lung disease. Respirology. 2024. https://doi.org/10.1111/resp.14848.
24. Zeng KF, Wang HJ, Deng B, et al. Ethyl ferulate suppresses post-myocardial infarction myocardial fibrosis by inhibiting transforming growth factor receptor 1. Phytomedicine. 2023;121: 155118. https://doi.org/10.1016/j.phymed.2023.155118.
25. Cao Y, Su H, Zeng J, et al. Integrin β8 prevents pericyte-myofibroblast transition and renal fibrosis through inhibiting the tgf-β1/tgfbr1/smad3 pathway in diabetic kidney disease. Transl Res. 2024;265:36–50. https://doi.org/10.1016/j.trsl.2023.10.007.
26. Zhang Z, Gao Y, Xu MQ, et al. Mir-181a regulate porcine preadipocyte differentiation by targeting tgfbr1. Gene. 2019;681:45–51. https://doi.org/10.1016/j.gene.2018.09.046.
27. Chen S, Luo Y, Cui L, et al. Mir-96-5p regulated tgf-β/smad signaling pathway and suppressed endometrial cell viability and migration via targeting tgfbr1. Cell Cycle. 2020;19(14):1740–53. https://doi.org/10.1080/15384101.2020.1777804.

28. Yang L, Pang Y, Moses HL. TGF-beta and immune cells: An important regulatory axis in the tumor microenvironment and progression. Trends Immunol. 2010;31(6):220–7. https://doi.org/10.1016/j.it.2010.04.002.
29. Li MO, Flavell RA. TGF-beta: a master of all t cell trades. Cell. 2008;134(3):392–404. https://doi.org/10.1016/j.cell.2008.07.025.
30. Zhang XX, Liu Y, Xu SS, et al. Asiatic acid from cyclocarya paliurus regulates the autophagy-lysosome system via directly inhibiting tgf-β type i receptor and ameliorates diabetic nephropathy fibrosis. Food Funct. 2022;13(10):5536–46. https://doi.org/10.1039/d1fo02445k.
31. You Y, Gao C, Wu J, et al. Enhanced expression of ark5 in hepatic stellate cell and hepatocyte synergistically promote liver fibrosis. Int J Mol Sci. 2022. https://doi.org/10.3390/ijms232113084.
32. Wang Q, Tao Y, Xie H, et al. Microrna-101 inhibits renal tubular epithelial-to-mesenchymal transition by targeting tgf-β1 type i receptor. Int J Mol Med. 2021. https://doi.org/10.3892/ijmm.2021.4952.
33. Ye Z, Hu Y. Tgf-β1: Gentlemanly orchestrator in idiopathic pulmonary fibrosis (review). Int J Mol Med. 2021. https://doi.org/10.3892/ijmm.2021.4965.
34. Fernández-Francos S, Eiro N, Costa LA, et al. Mesenchymal stem cells as a cornerstone in a galaxy of intercellular signals: basis for a new era of medicine. Int J Mol Sci. 2021. https://doi.org/10.3390/ijms22073576.
35. Andrzejewska A, Lukomska B, Janowski M. Concise review: mesenchymal stem cells: from roots to boost. Stem Cells. 2019;37(7):855–64. https://doi.org/10.1002/stem.3016.
36. Rani S, Ryan AE, Griffin MD, et al. Mesenchymal stem cell-derived extracellular vesicles: toward cell-free therapeutic applications. Mol Ther. 2015;23(5):812–23. https://doi.org/10.1038/mt.2015.44.
37. Van Griensven M, Balmayor ER. Extracellular vesicles are key players in mesenchymal stem cells' dual potential to regenerate and modulate the immune system. Adv Drug Deliv Rev. 2024;207:115203. https://doi.org/10.1016/j.addr.2024.115203.
38. Liu P, Yang S, Shao X, et al. Mesenchymal stem cells-derived exosomes alleviate acute lung injury by inhibiting alveolar macrophage pyroptosis. Stem Cells Transl Med. 2024. https://doi.org/10.1093/stcltm/szad094.
39. Farahmand Y, Nabiuni M, Vafaei Mastanabad M, et al. The exo-microrna (mirna) signaling pathways in pathogenesis and treatment of stroke diseases: emphasize on mesenchymal stem cells (MSCS). Cell Biochem Funct. 2024;42(2):e3917. https://doi.org/10.1002/cbf.3917.
40. Hammond SM. An overview of micrornas. Adv Drug Deliv Rev. 2015;87:3–14. https://doi.org/10.1016/j.addr.2015.05.001.
41. Xiao K, He W, Guan W, et al. Mesenchymal stem cells reverse EMT process through blocking the activation of nf-κb and hedgehog pathways in LPS-induced acute lung injury. Cell Death Dis. 2020;11(10):863. https://doi.org/10.1038/s41419-020-03034-3.
42. Zhou J, Lin Y, Kang X, et al. Microrna-186 in extracellular vesicles from bone marrow mesenchymal stem cells alleviates idiopathic pulmonary fibrosis via interaction with sox4 and dkk1. Stem Cell Res Ther. 2021;12(1):96. https://doi.org/10.1186/s13287-020-02083-x.
43. Cao L, Qin P, Zhang J, et al. Lncrna pvt1 suppresses the progression of renal fibrosis via inactivation of tgf-β signaling pathway. Drug Des Devel Ther. 2020;14:3547–57. https://doi.org/10.2147/dddt.S245244.
44. Zhao H, Guo Y, Sun Y, et al. Mir-181a/b-5p ameliorates inflammatory response in monocrotaline-induced pulmonary arterial hypertension by targeting endocan. J Cell Physiol. 2020;235(5):4422–33. https://doi.org/10.1002/jcp.29318.
45. Liu R, Zhang X, Fan Z, et al. Human amniotic mesenchymal stem cells improve the follicular microenvironment to recover ovarian function in premature ovarian failure mice. Stem Cell Res Ther. 2019;10(1):299. https://doi.org/10.1186/s13287-019-1315-9.
46. Xiao S, Huang G, Wei Z, et al. Il-10 gene-modified human amniotic mesenchymal stem cells augment regenerative wound healing by multiple synergistic effects. Stem Cells Int. 2019;2019:9158016. https://doi.org/10.1155/2019/9158016.
47. Zhang LT, Liu RM, Luo Y, et al. Hyaluronic acid promotes osteogenic differentiation of human amniotic mesenchymal stem cells via the tgf-β/smad signalling pathway. Life Sci. 2019;232: 116669. https://doi.org/10.1016/j.lfs.2019.116669.
48. He F, Wang Y, Li Y, et al. Human amniotic mesenchymal stem cells alleviate paraquat-induced pulmonary fibrosis in rats by inhibiting the inflammatory response. Life Sci. 2020;243: 117290. https://doi.org/10.1016/j.lfs.2020.117290.
49. Zhang C, Zhu X, Hua Y, et al. Yy1 mediates tgf-β1-induced emt and pro-fibrogenesis in alveolar epithelial cells. Respir Res. 2019;20(1):249. https://doi.org/10.1186/s12931-019-1223-7.
50. Kim BN, Ahn DH, Kang N, et al. Tgf-β induced emt and stemness characteristics are associated with epigenetic regulation in lung cancer. Sci Rep. 2020;10(1):10597. https://doi.org/10.1038/s41598-020-67325-7.
51. Gui Y, Sun J, You W, et al. Glycyrrhizin suppresses epithelial-mesenchymal transition by inhibiting high-mobility group box1 via the tgf-β1/smad2/3 pathway in lung epithelial cells. PeerJ. 2020;8: e8514. https://doi.org/10.7717/peerj.8514.
52. Xu X, Ma C, Wu H, et al. Fructose induces pulmonary fibrotic phenotype through promoting epithelial-mesenchymal transition mediated by ros-activated latent tgf-β1. Front Nutr. 2022;9: 850689. https://doi.org/10.3389/fnut.2022.850689.
53. Chang YH, Kumar VB, Wen YT, et al. Induction of human umbilical mesenchymal stem cell differentiation into retinal pigment epithelial cells using a transwell-based co-culture system. Cell Transplant. 2022;31:9636897221085900. https://doi.org/10.1177/09636897221085901.
54. Wang F, Zhu J, Zheng J, et al. Mir-210 enhances mesenchymal stem cell-modulated neural precursor cell migration. Mol Med Rep. 2020;21(6):2405–14. https://doi.org/10.3892/mmr.2020.11065.
55. Chen HC, Awale S, Wu CP, et al. Co-cultured bone marrow mesenchymal stem cells repair thioacetamide-induced hepatocyte damage. Cell Biol Int. 2020;44(12):2459–72. https://doi.org/10.1002/cbin.11453.
56. Gul A, Yang F, Xie C, et al. Pulmonary fibrosis model of mice induced by different administration methods of bleomycin. BMC Pulm Med. 2023;23(1):91. https://doi.org/10.1186/s12890-023-02349-z.
57. Sun T, Li H, Zhang Y, et al. Inhibitory effects of 3-cyclopropylmethoxy-4-(difluoromethoxy) benzoic acid on TGF-β1-induced epithelial-mesenchymal transformation of in vitro and bleomycin-induced pulmonary fibrosis in vivo. Int J Mol Sci. 2023. https://doi.org/10.3390/ijms24076172.
58. Mishra SK, Khushu S, Singh AK, et al. Homing and tracking of iron oxide labelled mesenchymal stem cells after infusion in traumatic brain injury mice: a longitudinal in vivo mri study. Stem Cell Rev Rep. 2018;14(6):888–900. https://doi.org/10.1007/s12015-018-9828-7.
59. Schol J, Sakai D, Warita T, et al. Homing of vertebral-delivered mesenchymal stromal cells for degenerative intervertebral discs repair - an in vivo proof-of-concept study. JOR Spine. 2023;6(1): e1228. https://doi.org/10.1002/jsp2.1228.
60. Guo Z, Zhang Y, Yan F. Potential of mesenchymal stem cell-based therapies for pulmonary fibrosis. DNA Cell Biol. 2022;41(11):951–65. https://doi.org/10.1089/dna.2022.0327.
61. Li X, Li X, Yang J, et al. Living and injectable porous hydrogel microsphere with paracrine activity for cartilage regeneration. Small. 2023;19(17): e2207211. https://doi.org/10.1002/smll.202207211.
62. Fernandes SS, Limaye LS, Kale VP. Differentiated cells derived from hematopoietic stem cells and their applications in translational medicine. Adv Exp Med Biol. 2021;1347:29–43. https://doi.org/10.1007/5584_2021_644.
63. Alvites R, Branquinho M, Sousa AC, et al. Mesenchymal stem/stromal cells and their paracrine activity-immunomodulation mechanisms and how to influence the therapeutic potential. Pharmaceutics. 2022. https://doi.org/10.3390/pharmaceutics14020381.
64. Son D, Zheng J, Kim IY, et al. Human induced neural stem cells support functional recovery in spinal cord injury models. Exp Mol Med. 2023;55(6):1182–92. https://doi.org/10.1038/s12276-023-01003-2.
65. Cao X, Gu L, Zhang Z, et al. Mir-181a-5p restrains non-small cell lung cancer cell invasion and migration by regulating the gtse1/p53/nf-κb axis. Cells Tissues Organs. 2022. https://doi.org/10.1159/000525432.
66. Sun CX, Liu BJ, Su Y, et al. Mir-181a promotes cell proliferation and migration through targeting klf15 in papillary thyroid cancer. Clin Transl Oncol. 2022;24(1):66–75. https://doi.org/10.1007/s12094-021-02670-1.
67. Wei JJ, Tang L, Chen LL, et al. Mesenchymal stem cells attenuates tgf-β1-induced emt by increasing hgf expression in hk-2 cells. Iran J Public Health. 2021;50(5):908–18. https://doi.org/10.18502/ijph.v50i5.6108.

68. Brownfield DG, de Arce AD, Ghelfi E, et al. Alveolar cell fate selection and lifelong maintenance of at2 cells by fgf signaling. Nat Commun. 2022;13(1):7137. https://doi.org/10.1038/s41467-022-34059-1.
69. Han MM, He XY, Tang L, et al. Nanoengineered mesenchymal stem cell therapy for pulmonary fibrosis in young and aged mice. Sci Adv. 2023;9(29):eadg5358. https://doi.org/10.1126/sciadv.adg5358.
70. Xu C, Feng C, Huang P, et al. Tnfα and ifnγ rapidly activate pi3k-akt signaling to drive glycolysis that confers mesenchymal stem cells enhanced anti-inflammatory property. Stem Cell Res Ther. 2022;13(1):491. https://doi.org/10.1186/s13287-022-03178-3.
71. Chen J, Crawford R, Chen C, et al. The key regulatory roles of the pi3k/akt signaling pathway in the functionalities of mesenchymal stem cells and applications in tissue regeneration. Tissue Eng Part B Rev. 2013;19(6):516–28. https://doi.org/10.1089/ten.TEB.2012.0672.
72. Ding X, Xu X, He XF, et al. Muscleblind-like 1 antisense rna 1 inhibits cell proliferation, invasion, and migration of prostate cancer by sponging mir-181a-5p and regulating pten/pi3k/akt/mtor signaling. Bioengineered. 2021;12(1):803–14. https://doi.org/10.1080/21655979.2021.1890383.
73. Giarratana AO, Prendergast CM, Salvatore MM, et al. Tgf-β signaling: Critical nexus of fibrogenesis and cancer. J Transl Med. 2024;22(1):594. https://doi.org/10.1186/s12967-024-05411-4.
74. Sun T, Vander Heiden JA, Gao X, et al. Isoform-selective tgf-β3 inhibition for systemic sclerosis. Med. 2024;5(2):132-147.e137. https://doi.org/10.1016/j.medj.2023.12.011.
75. Pelaia C, Vatrella A, Gallelli L, et al. Role of p38 mitogen-activated protein kinase in asthma and copd: pathogenic aspects and potential targeted therapies. Drug Des Devel Ther. 2021;15:1275–84. https://doi.org/10.2147/dddt.S300988.
76. Kasuya Y, Kim JD, Hatano M, et al. Pathophysiological roles of stress-activated protein kinases in pulmonary fibrosis. Int J Mol Sci. 2021. https://doi.org/10.3390/ijms22116041.
77. Wang Y, Han Y, Shang K, et al. Kokusaginine attenuates renal fibrosis by inhibiting the pi3k/akt signaling pathway. Biomed Pharmacother. 2024;175: 116695. https://doi.org/10.1016/j.biopha.2024.116695.
78. Shamsan E, Almezgagi M, Gamah M, et al. The role of pi3k/akt signaling pathway in attenuating liver fibrosis: A comprehensive review. Front Med (Lausanne). 2024;11:1389329. https://doi.org/10.3389/fmed.2024.1389329.
79. Romero Y, Bueno M, Ramirez R, et al. Mtorc1 activation decreases autophagy in aging and idiopathic pulmonary fibrosis and contributes to apoptosis resistance in IPF fibroblasts. Aging Cell. 2016;15(6):1103–12. https://doi.org/10.1111/acel.12514.
80. Choi YY, Seok JI, Hwang JI, et al. Co-administration of everolimus and n-acetylcysteine attenuates hepatic stellate cell activation and hepatic fibrosis. Am J Transl Res. 2020;12(6):2627–39.
81. Platé M, Guillotin D, Chambers RC. The promise of mtor as a therapeutic target pathway in idiopathic pulmonary fibrosis. Eur Respir Rev. 2020. https://doi.org/10.1183/16000617.0269-2020.
82. Gumede DB, Abrahamse H, Houreld NN. Targeting wnt/β-catenin signaling and its interplay with tgf-β and notch signaling pathways for the treatment of chronic wounds. Cell Commun Signal. 2024;22(1):244. https://doi.org/10.1186/s12964-024-01623-9.
83. Li F, Wang X, Shi J, et al. Anti-inflammatory effect of dental pulp stem cells. Front Immunol. 2023;14:1284868. https://doi.org/10.3389/fimmu.2023.1284868.
84. Shi Y, Wang Y, Li Q, et al. Immunoregulatory mechanisms of mesenchymal stem and stromal cells in inflammatory diseases. Nat Rev Nephrol. 2018;14(8):493–507. https://doi.org/10.1038/s41581-018-0023-5.
85. Chan M, Liu Y. Function of epithelial stem cell in the repair of alveolar injury. Stem Cell Res Ther. 2022;13(1):170. https://doi.org/10.1186/s13287-022-02847-7.
86. Taherian M, Bayati P, Mojtabavi N. Stem cell-based therapy for fibrotic diseases: Mechanisms and pathways. Stem Cell Res Ther. 2024;15(1):170. https://doi.org/10.1186/s13287-024-03782-5.
87. Shan L, Wang F, Zhai D, et al. Matrix metalloproteinases induce extracellular matrix degradation through various pathways to alleviate hepatic fibrosis. Biomed Pharmacother. 2023;161: 114472. https://doi.org/10.1016/j.biopha.2023.114472.
88. Asgari R, Mehran YZ, Weber HM, et al. Management of oxidative stress for cell therapy through combinational approaches of stem cells, antioxidants, and photobiomodulation. Eur J Pharm Sci. 2024;196:106715. https://doi.org/10.1016/j.ejps.2024.106715.
89. Mabotuwana NS, Rech L, Lim J, et al. Paracrine factors released by stem cells of mesenchymal origin and their effects in cardiovascular disease: a systematic review of pre-clinical studies. Stem Cell Rev Rep. 2022;18(8):2606–28. https://doi.org/10.1007/s12015-022-10429-6.
90. Zheng J, Park K, Jang J, et al. Utilizing stem cell-secreted molecules as a versatile toolbox for skin regenerative medicine. J Control Release. 2024;370:583–99. https://doi.org/10.1016/j.jconrel.2024.05.009.
91. Bao H, Wu M, Xing J, et al. Enzyme-like nanoparticle-engineered mesenchymal stem cell secreting hgf promotes visualized therapy for idiopathic pulmonary fibrosis in vivo. Sci Adv. 2024;10(34):eadq0703. https://doi.org/10.1126/sciadv.adq0703.
92. Hassanzadeh A, Shamlou S, Yousefi N, et al. Genetically-modified stem cell in regenerative medicine and cancer therapy; a new era. Curr Gene Ther. 2022;22(1):23–39. https://doi.org/10.2174/1566523221666210707125342.
93. Matsuzaka Y, Yashiro R. Current strategies and therapeutic applications of mesenchymal stem cell-based drug delivery. Pharmaceuticals (Basel). 2024. https://doi.org/10.3390/ph17060707.
94. Li Q, Zhang F, Fu X, et al. Therapeutic potential of mesenchymal stem cell-derived exosomes as nanomedicine for peripheral nerve injury. Int J Mol Sci. 2024. https://doi.org/10.3390/ijms25147882.
95. Mei R, Wan Z, Yang C, et al. Advances and clinical challenges of mesenchymal stem cell therapy. Front Immunol. 2024;15:1421854. https://doi.org/10.3389/fimmu.2024.1421854.
96. Giugni FR, Giugni MOV, Pinesi HT, et al. Safety and efficacy of adipose-derived mesenchymal stem cell therapy for ischemic heart disease: a systematic review. Arq Bras Cardiol. 2024;121(9): e20230830. https://doi.org/10.36660/abc.20230830.
97. Afkhami H, Mahmoudvand G, Fakouri A, et al. New insights in application of mesenchymal stem cells therapy in tumor microenvironment: pros and cons. Front Cell Dev Biol. 2023;11:1255697. https://doi.org/10.3389/fcell.2023.1255697.
98. Li H, Wang Y, Zhu G, et al. Application progress of single-cell sequencing technology in mesenchymal stem cells research. Front Cell Dev Biol. 2023;11:1336482. https://doi.org/10.3389/fcell.2023.1336482.
99. Masterson CH, Curley GF, Laffey JG. Modulating the distribution and fate of exogenously delivered mscs to enhance therapeutic potential: Knowns and unknowns. Intensive Care Med Exp. 2019;7(Suppl 1):41. https://doi.org/10.1186/s40635-019-0235-4.
100. Česnik AB, Švajger U. The issue of heterogeneity of msc-based advanced therapy medicinal products-a review. Front Cell Dev Biol. 2024;12:1400347. https://doi.org/10.3389/fcell.2024.1400347.
101. Zhang B, Lai RC, Sim WK, et al. An assessment of administration route on msc-sev therapeutic efficacy. Biomolecules. 2024. https://doi.org/10.3390/biom14060622.

Publisher's Note